Design Strategies of Tumor-Targeted Delivery Systems Based on 2D Nanomaterials

Lin Ding, Minli Liang, Chenchen Li, Xinting Ji, Junfeng Zhang, Weifen Xie, Rui L. Reis, Fu-Rong Li,* Shuo Gu,* and Yanli Wang*

Conventional chemotherapy and radiotherapy are nonselective and nonspecific for cell killing, causing serious side effects and threatening the lives of patients. It is of great significance to develop more accurate tumor-targeting therapeutic strategies. Nanotechnology is in a leading position to provide new treatment options for cancer, and it has great potential for selective targeted therapy and controlled drug release. 2D nanomaterials (2D NMs) have broad application prospects in the field of tumor-targeted delivery systems due to their special structure-based functions and excellent optical, electrical, and thermal properties. This review emphasizes the design strategies of tumor-targeted delivery systems based on 2D NMs from three aspects: passive targeting, active targeting, and tumor-microenvironment targeting, in order to promote the rational application of 2D NMs in clinical practice.

1. Introduction

Globally, cancer remains one of the most serious diseases threatening human health. Common anticancer drugs are distributed throughout the human body when orally administered or injected, causing nonspecific damage to normal cells and tissues.[1] Radiotherapy uses large doses of high-energy particle beams to kill cancer cells and cause serious damage to surrounding normal tissues.[2] The development of friendly tumor-targeted therapies enables the specific killing of cancer cells while reducing damage to normal cells. Tumor-targeted therapy aims to improve the tumor-specific targeting of therapeutic reagents, accurately attacking tumors and minimizing damage to normal cells. Such therapies are expected to improve the survival rate of cancer patients.

In recent years, the vigorous development of nanotechnology has revealed the advantages and potential of nanomaterial-based platforms in the fields of drug delivery, diagnostics, and cancer treatment. Various types of nanomaterials such as 0D nanoparticles and nanodots, 1D nanowires and nanotubes, 2D nanosheets, and 3D nanostents play key roles in energy storage, biomedicine, electronic technology, and other fields. Among them, 2D nanomaterials (2D NMs) have attracted attention due to their excellent physical and chemical properties, and they have unique advantages and application prospects in the field of precision targeted-delivery systems for tumors.

2D NMs refer to materials in which electrons can move freely on the nanoscale in only two dimensions (plane motion).

L. Ding, X. Ji, S. Gu, Y. Wang
School of Pharmaceutical Sciences and The First Affiliated Hospital
Hainan Medical University
Haikou 570228, P. R. China
E-mail: gushuo007@hainmc.edu.cn; wangyanli@staff.shu.edu.cn

L. Ding, M. Liang, F.-R. Li
The First Affiliated Hospital (Shenzhen People's Hospital)
Southern University of Science and Technology
Shenzhen 518055, China
E-mail: lifurong@mail.sustech.edu.cn

L. Ding, M. Liang, F.-R. Li
Translational Medicine Collaborative Innovation Center
Shenzhen People's Hospital (The First Affiliated Hospital
Southern University of Science and Technology
The Second Clinical Medical College of Jinan University)
Shenzhen, Guangdong 518055, China

L. Ding, M. Liang, F.-R. Li
Guangdong Engineering Technology Research Center
of Stem Cell and Cell Therapy
Shenzhen Key Laboratory of Stem Cell Research
and Clinical Transformation
Shenzhen Immune Cell Therapy Public Service Platform
Shenzhen 518020, China

C. Li, J. Zhang, Y. Wang
Tumor Precision Targeting Research Center
School of Environmental and Chemical Engineering
Shanghai University
Shanghai 200444, P. R. China

W. Xie
Department of Gastroenterology
Changzheng Hospital
Naval Medical University
Shanghai 200003, China

R. L. Reis
3B's Research Group
I3Bs-Research Institute on Biomaterials Biodegradables
and Biomimetics
University of Minho
Guimarães 4805-017, Portugal

**ADVANCED
SCIENCE NEWS**

www.advancedsciencenews.com

**small
methods**

www.small-methods.com

2D NMs are typically nanosheets with a layer thickness of <100 nm formed by single atoms or polyatoms.[3] Since graphene was first reported in 2004, this single-layer sheet-like 2D NM has aroused great interest.[4] In recent years, a number of new types of 2D NMs have been reported, including 2D metal–organic frameworks (MOFs),[5] layered double hydroxides (LDHs),[6–11] nitrides and carbonitrides (MXenes),[12] transition metal oxides (TMOs),[13] transition-metal dichalcogenides (TMDs),[14] single-element 2D NMs (e.g., black phosphorus (BP)),[15] silicon (Si) nanosheets,[16] antimonene (AM) nanosheets,[17] and nonmetallic 2D NMs (e.g., hexagonal boron nitride (h-BN)).[18] The unique structure of 2D NMs imparts excellent physical, thermal, electrical, and optical properties. This unique structure, which gives the 2D NMs obvious advantages as tumor-targeted delivery therapeutics, includes:[19] i) a large specific surface area, which imparts high loading capacity and can increase the delivery dose of anticancer drugs; ii) a single-layer structure that simplifies forming covalent and noncovalent bonds with other substances, allowing flexibility in targeted surface modification; iii) an excellent photothermal conversion ability, allowing 2D NMs to be used directly as local photothermal treatment (PTT) reagents; and iv) good biocompatibility and low toxicity, which can accelerate clinical application (**Figure 1**).

Currently, based on tumor-related features, various nanomaterial targeted-therapy strategies have been developed. In general, there are three main strategies: passive targeting, active targeting, and related targeting strategies for the tumor microenvironment (TME). The functional advantages of 2D NMs are expected to assist the development of targeted tumor therapies. Therefore, this review provides a detailed summary of tumor-targeted therapy strategies designed using 2D NMs in recent years, with the goal of promoting the rational application of 2D NMs in clinical tumor-targeted therapies.

2. Passive Targeting

In 1986, Matsumura and Maeda serendipitously found that anticancer proteins and polymer-binding compounds accumulated in tumor sites. The reason for this finding was shown to be hyperplasia of blood vessels at the tumor site, with large spaces between blood vessels and no lymphatic reflux, leading to leakage of macromolecules into the
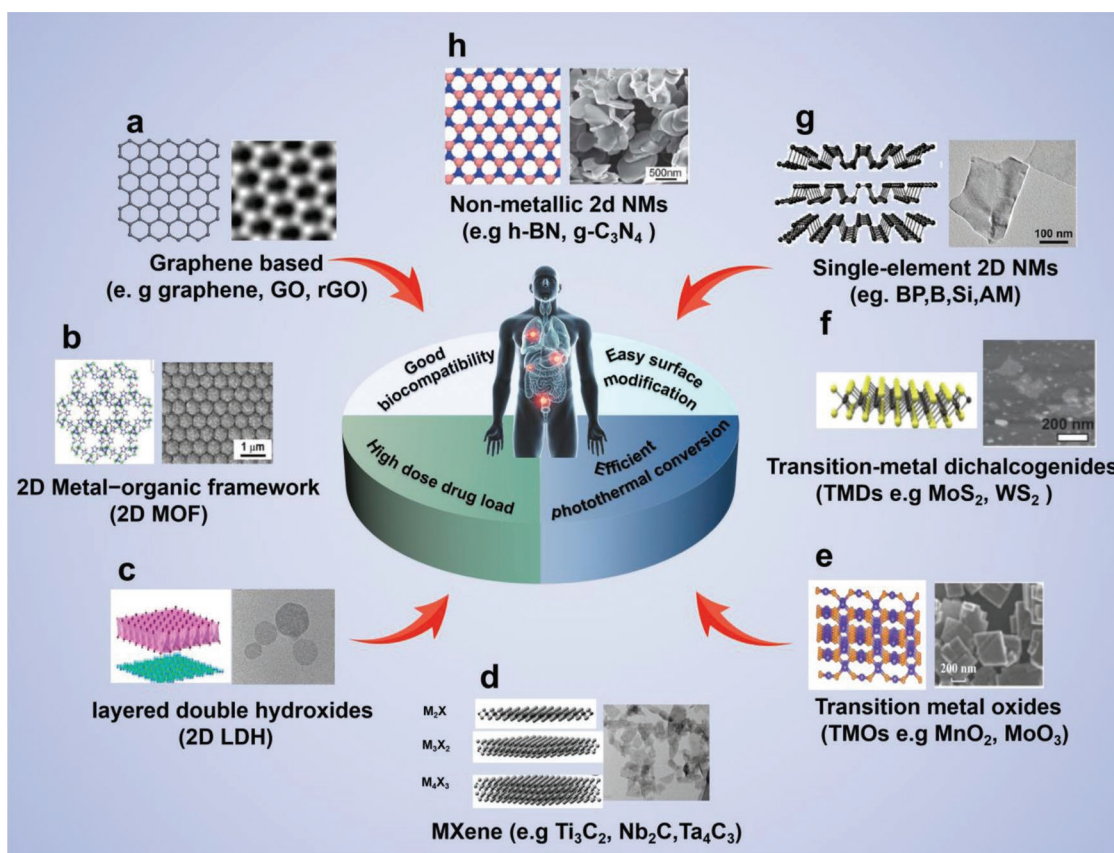
Figure 1. Classification of 2D NMs and their advantages in tumor targeted delivery systems. a) Graphene based. Reproduced with permission.[4] Copyright 2021, Elsevier. b) 2D MOFs. Reproduced with permission.[5] Copyright 2016, American Chemical Society. c) LDHs. Reproduced with permission.[6] Copyright 2022, Wiley-VCH. d) MXenes. Reproduced with permission.[12] Copyright 2018, American Chemical Society. e) TMOs. Reproduced with permission.[13] Copyright 2018, Springer. f) TMDs. Reproduced with permission.[14] Copyright 2014, Wiley-VCH. g) Single-element 2D NMs. Reproduced with permission.[15] Copyright 2018, Wiley-VCH. h) Nonmetallic 2D NMs. Reproduced with permission.[18] Copyright 2011, The Royal Society of Chemistry.

**ADVANCED
SCIENCE NEWS**

www.advancedsciencenews.com

**small
methods**

www.small-methods.com
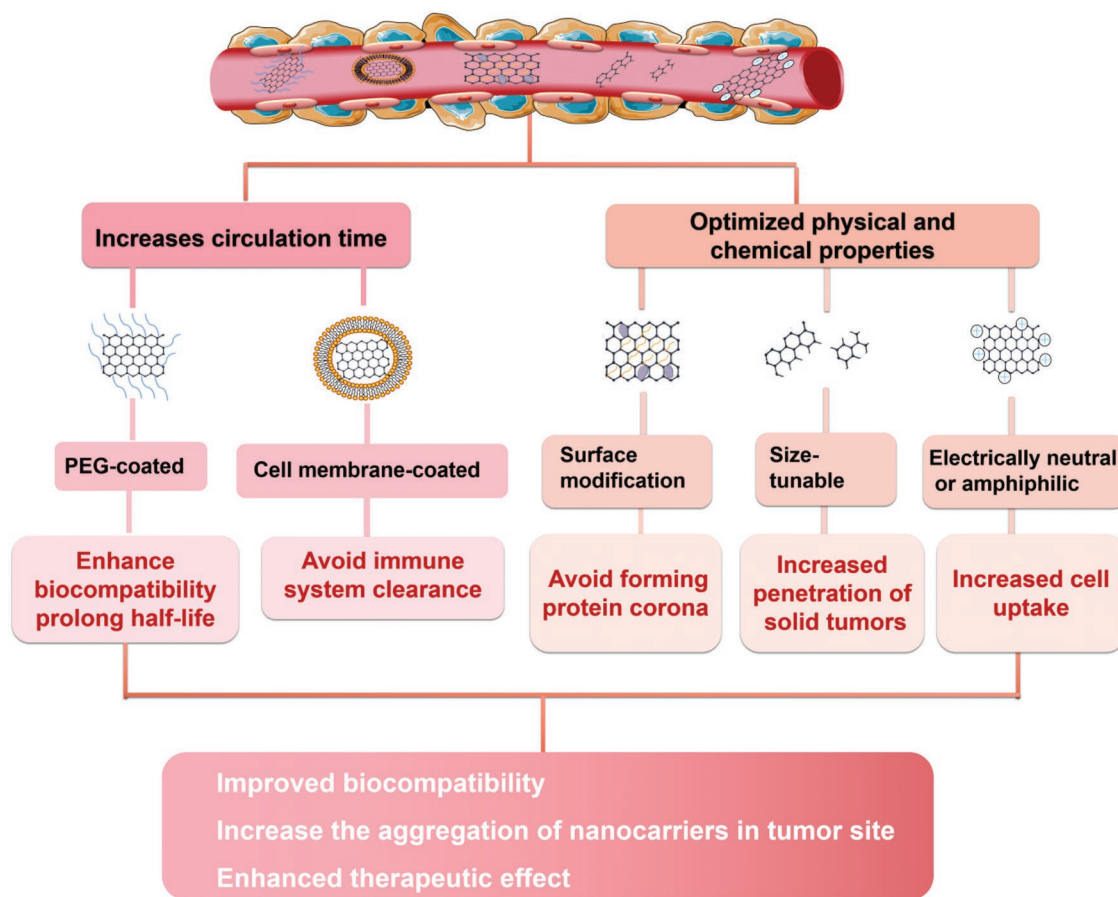
Figure 2. Strategies to improve passive targeting efficiency.

tumor site through the blood vessels.[20] This is known as the enhanced permeability and retention effect (EPR effect) or passive targeting. Leaking vessels allow macromolecules larger than 40 kDa and nanosystems to selectively accumulate at the tumor site, while small molecule drugs are not suitable for this. Thus, the EPR effect opens the door for nanomaterials to target tumors.[21]

After several decades, the EPR effect has become the "gold standard" for the targeted design of nanomaterials. A variety of nanomedicines based on the EPR effect have been applied in clinical practice, such as Doxil, Abraxane, Marqibo, DaunoXome, and Onivyde in the US; Myocet and Mepact in Europe; Genexol-PM in Korea; and SMANCS in Japan.[22] Although the median injected dose (ID) of nanocarriers reaching tumors has been reported to be only 0.7% (including both passive and active targeting), this delivery efficiency is still higher than that of conventional anticancer drugs.[23,24] For example, one study showed that nanocarriers loaded with paclitaxel had a delivery efficiency of 0.6% ID, while free paclitaxel had a delivery efficiency of only 0.2% ID.[25] Moreover, clinical data suggest that EPR effect-based nanomedicines improve patient survival compared to free drugs.[26] This clinical evidence suggests that the EPR effect is real and effective in improving oncology treatment, but there is still considerable room for improvement.

The effectiveness of the EPR effect is related to several key factors. First, the circulation time of the nanomedicine directly determines the tumor-targeting ratio.[21] Increasing the circulation time of the nanosystem could effectively improve the passive targeting efficiency of the nanomedicine at the tumor site. Second, the EPR effect is closely related to the size of the nanosystem. The pore size of tumor vessels ranges from 200 nm to 1.2 µm. Nanoparticles with a diameter of less than 6 nm are cleared by the kidneys, while particles larger than 500 nm are captured by the reticuloendothelial system. Consequently, the nanosystem should be designed with full consideration of the impact of particle size.[27] Third, the surface properties of nanomaterials, such as surface charge and modification, also play an important role in tumor targeting.[28] Therefore, the design of passive targeting based on the EPR effect should be considered from all aspects. This section further describes methods to increase passive targeting efficiency (**Figure 2**).

2.1. Increasing Circulation Time

2.1.1. Polyethylene Glycol (PEG)-Coated 2D NMs

Traditional small-molecule anticancer drugs possess disadvantages such as poor water solubility, a short half-life, lack of

selectivity, and high toxicity.[29] Nanomaterial-based drug delivery systems have the ability to increase the circulation time of drugs, improve drug metabolism, and reduce side effects to improve the targeted therapeutic effect. Researchers have developed a variety of strategies to increase the circulation time of nanosystems.

PEG has been approved by the Food and Drug Administration for use as a carrier of food and medicine. PEG modification is the most common method to increase carrier circulation time. For example, Pan et al. reported on indocyanine green (ICG)-loaded PEG-modified BP nanosheets for imaging-guided cancer therapy (**Figure 3**a). After coincubation of ICG and ICP@BPNS-PEG with 4T1 cells for 1 h, it was found that the intracellular fluorescence intensity in the ICP@BPNS-PEG group was twice as high as that in the ICG group, indicating that ICP@BPNS-PEG had a high EPR effect that could improve binding to tumor cells and uptake of ICG (Figure 3b). In vivo imaging results showed that ICP@BPNS-PEG had a longer circulation time and an increase in the effective accumulation of vector in the tumor site (Figure 3c). Combined with laser treatment, ICP@BPNS-PEG could significantly inhibit growth of the tumor (Figure 3d).[30] Ji et al. constructed a sandwich-structure vermiculite 2D nanosheet (FCLs) for cancer theranostics. As shown in Figure 3e, PEG modification greatly increased the dispersity of the carrier, making it more favorable for biological applications. Biological distribution of FCL-PEG-Cy7 NSs in major organs and tumors 24 h after injection was observed. Fluorescence imaging (Figure 3f) and photoacoustic

imaging (Figure 3g) showed that FCL-PEG-Cy7 NSs had a longer cycle time than free Cy7, and FCL-PEG-Cy7 NSs had a high accumulation in tumor sites. The injection of FCL-PEG NSs and 658 nm laser irradiation significantly and specifically induced the production of reactive oxygen species (ROS) levels in tumors, resulting in high tumor cytotoxicity (Figure 3h).[31] Some other examples of surface modification of 2D NMs using PEG are shown in **Table 1**.[165–173]

PEG modification can effectively improve the half-life of drug delivery vectors, increase biocompatibility, and improve the effective accumulation of drug delivery vectors at tumor sites, thus enhancing treatment efficacy.

2.1.2. Cell Membrane-Coated 2D NMs

The clearance of nanoparticles by the immune system is a huge barrier for drug delivery, and in recent years, a biomimetic strategy has been developed that uses "camouflage modification" to evade immune clearance. As an integral part of the body, cell membranes can retain cell surface antigens, have excellent biocompatibility, and are not easily recognized by the immune system.[32]

The common sources of cell membranes are immune cells, red blood cells (RBCs), tumor cells, stem cells, and bacteria (**Figure 4**a). A transmembrane protein CD47 expressed on the surface of RBCs helps prevent macrophage uptake by selectively
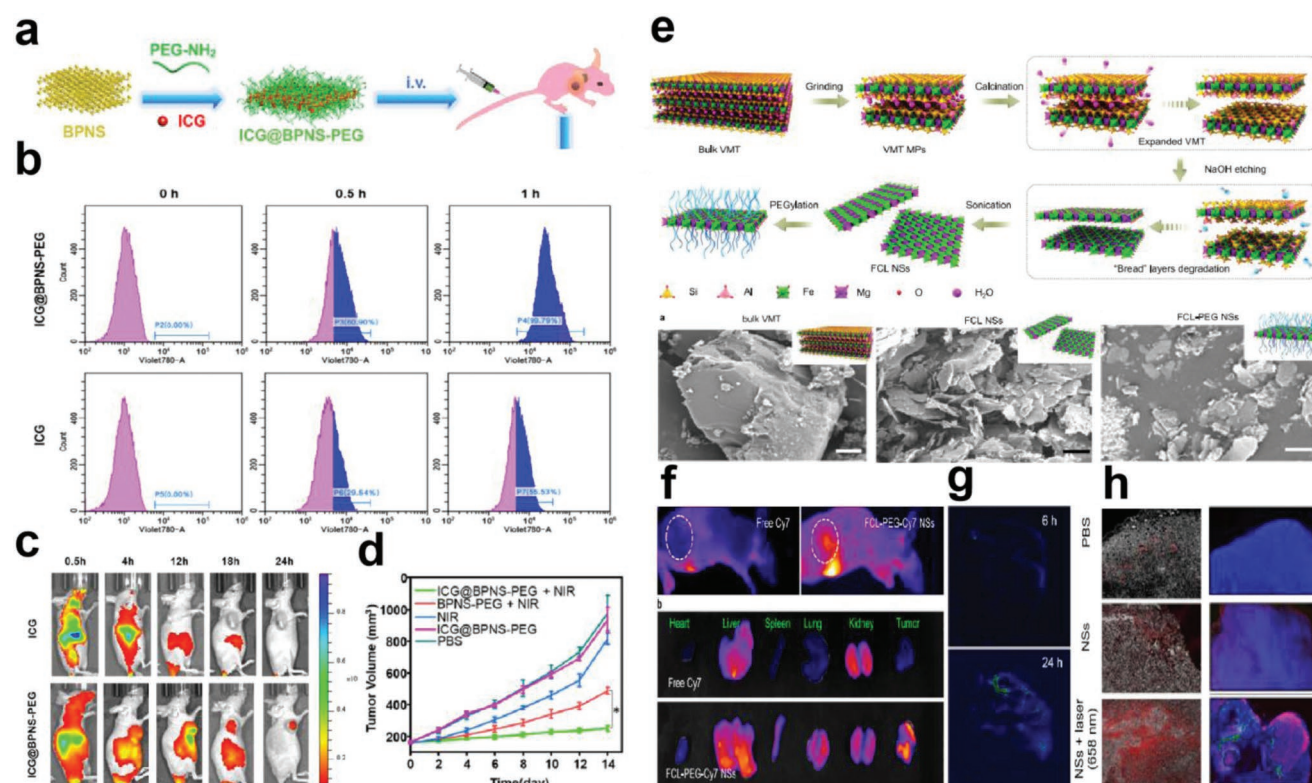
Figure 3. PEG-coated 2D NMs enhances passive targeted therapy efficiency. a–d) ICP@BPNS-PEG promotes uptake of tumor cells, increases in vivo circulation time, tumor site aggregation, and tumor ablation. Reproduced with permission.[30] Copyright 2021, American Chemical Society. e–h) FCL-PEG-Cy7 NSs enhances biocompatibility, induces tumor ROS production, and induces tumor apoptosis. Reproduced with permission.[31] Copyright 2021, Springer Nature.

Table 1. PEG-coated 2D NMs to increase passive targeting efficiency.

PEG modification	Treatment strategies	Results
2D PEG–CuFe$_2$S$_3$	PTT and chemotherapy	Improve biocompatibility, long circulation time, excellent photothermal conversion efficiency (−55.86%), efficient synergistic antitumor activity[165]
2D PEG–Ti$_2$C	PTT	Good biocompatibility, minimal impact on nonmalignant cells, PEG-Ti$_2$C doses are 24 times lower than other MXene-based PTT agents[166]
2D PEG-Pd@Au nanoplate loading platinum(IV) prodrug c,c,t-[Pt(NH$_3$)$_2$Cl$_2$(O$_2$CCH$_2$CH$_2$CO$_2$H)$_2$]	PTT and chemotherapy	Excellent stability and efficient Pt(IV) prodrug loading, high tumor accumulation (29% ID g^{-1}), no recurrence in the synergistic treatment[167]
2D PEG-antimonene quantum dots (AMQDs)	PTT	Improve biocompatibility, higher photothermal conversion efficacy of 45.5%, rapid degradability[168]
2D PEG-GO loading acetaminophen (AMP), diclofenac (DIC), and methotrexate (MTX)	Chemotherapy	The MTX with the highest number of aromatic rings had the highest drug delivery efficiency, which was 95.6%, while the drugs with fewer aromatic rings were DIC (70.5%), AMP (65.5%).[169]
2D PEG–PLA–graphene loading anticancer drug paclitaxel	Chemotherapy	Decreases cytotoxicity, sustains prolonged PTX release for at least 19 days, significantly reduce the dose of drug[170]
2D mesoporous organosilicas (PMOs)–PEG–MoS$_2$–DOX	PTT and chemotherapy	High DOX loading, enhancement of tumor accumulation, enhanced the effect of combination therapy[171]
2D PEG–iron oxide nanoparticles (IONPs)–MoS$_2$	positron emission tomography imaging, photoacoustic tomography imaging, magnetic resonance imaging, and PTT	Three modality imaging guidance, and in vivo PTT, in animal tumor models to achieve effective tumor ablation[172]
2D PEG-conjugated Fe^{2+}-containing hydroxide nanosheet	Catalytic production of highly toxic ROS	Good degradability, safety, and high selectivity of tumor cells[173]

binding SIRPα expressed by macrophages as a "don't eat me" marker.[33] Platelets also express CD47 and thus avoid uptake by macrophages. Platelet membranes have additional proteins, such as CD55 and CD59 that suppress the immunological complement system. Therefore, nanoparticles coated with RBC/platelet membranes can prolong blood circulation and avoid macrophage clearance.[34] He et al. used RBC membrane camouflage 2D MoSe$_2$ nanosheets to effectively inhibit macrophage uptake by CD47 binding to SIRPα receptor (Figure 4b,c) and enhancing blood compatibility (Figure 4d). PTT results showed that the tumor growth inhibitory effect in the RBC-MoSe$_2$ group was the most significant, indicating that more RBC-MoSe$_2$ material gathered at the tumor site and stayed longer (Figure 4e,f). They also found that RBC-MoSe$_2$ triggered the release of tumor-associated antigens to activate cytotoxic T lymphocytes, and interestingly, tumor-associated macrophages were effectively reprogrammed into a tumor-killing M1 phenotype (Figure 4g–i). The volume of the primary tumor was measured within 21 days. After treatment with RBC-MoSe$_2$ nanosheets and irradiation with an 808 nm laser, the primary tumor almost disappeared, and the effect was equivalent to that of injection of an anti-PD-1 checkpoint inhibitor (Figure 4j).[35] Lu et al. reported on an RBC membrane-coated Nb$_2$C nanosheet treatment platform that demonstrated prolonged blood circulation and when combined with PTT, cleared all primary tumors.[36]

The overexpression of CD47 by cancer cells protects nanoparticles from immune scavenging, while the expression of Thomsen-Friedenreich antigen and E-cadherin by cancer cells allows nanoparticles to target conspecific tumors and increase adhesion and penetration of tumor tissues.[37] Zhang et al. developed cancer-cell-membrane-coated 2D LDH nanoparticles

(CMPEG/MnLDH) for tumor-enhanced magnetic resonance imaging (MRI) to achieve cell-specific targeting and deep tissue penetration (Figure 4k). To study the targeting and penetration ability of the same membrane-coated nanomaterials, 4T1 membrane-coated Dio-labeled PEG/MnLDH was incubated with 4T1 or MCF-7 cells. The 4T1 CM-PEG/MnLDH produced obvious fluorescence signals in the 4T1 cells, while the corresponding fluorescence signals in the MCF-7 cells were weak, indicating that the 4T1-coated material had high targeting ability to matched cells (Figure 4l,m). Next, the investigators studied tissue penetration; 4T1 CM-PEG/MnLDH was cocultured with 4T1 and MCF-7 3D tumor spheroids, and fluorescence signals in the tumor spheres at different depths were scanned by confocal microscopy. The results showed that the 4T1 CM-PEG/MnLDH penetrated deeply into the 4T1 tumor spheres. Strong fluorescence was still detected at a depth of 50 μm, but penetration of the MCF-7 cells was poor (Figure 4n). These results clearly showed that 4T1 CM-PEG/MnLDH had enhanced cell-specific targeting ability and excellent penetration performance. Mice were injected with PEG/MnLDH or 4T1 CM-PEG/MnLDH, and MRI results showed that tumor signals in the membrane-coated material group reached a higher level within 6 h than those in the group without membrane coating and remained high until 24 h. Moreover, the signal in the central tumor region of the 4T1 CM-PEG/MnLDH group was significantly higher than that of the PEG/MnLDH group (Figure 4o), which further confirmed the enhanced tissue penetration ability of the cancer cell membrane coating.[38] Zhang et al. reported on a composite cancer-cell-membrane-coated MnO$_2$ nanosheet that was also coated with gold nanorod-loaded doxorubicin (DOX). The cell membrane modification greatly improved the colloid stability of

ADVANCED
SCIENCE NEWS

www.advancedsciencenews.com

small
methods

www.small-methods.com
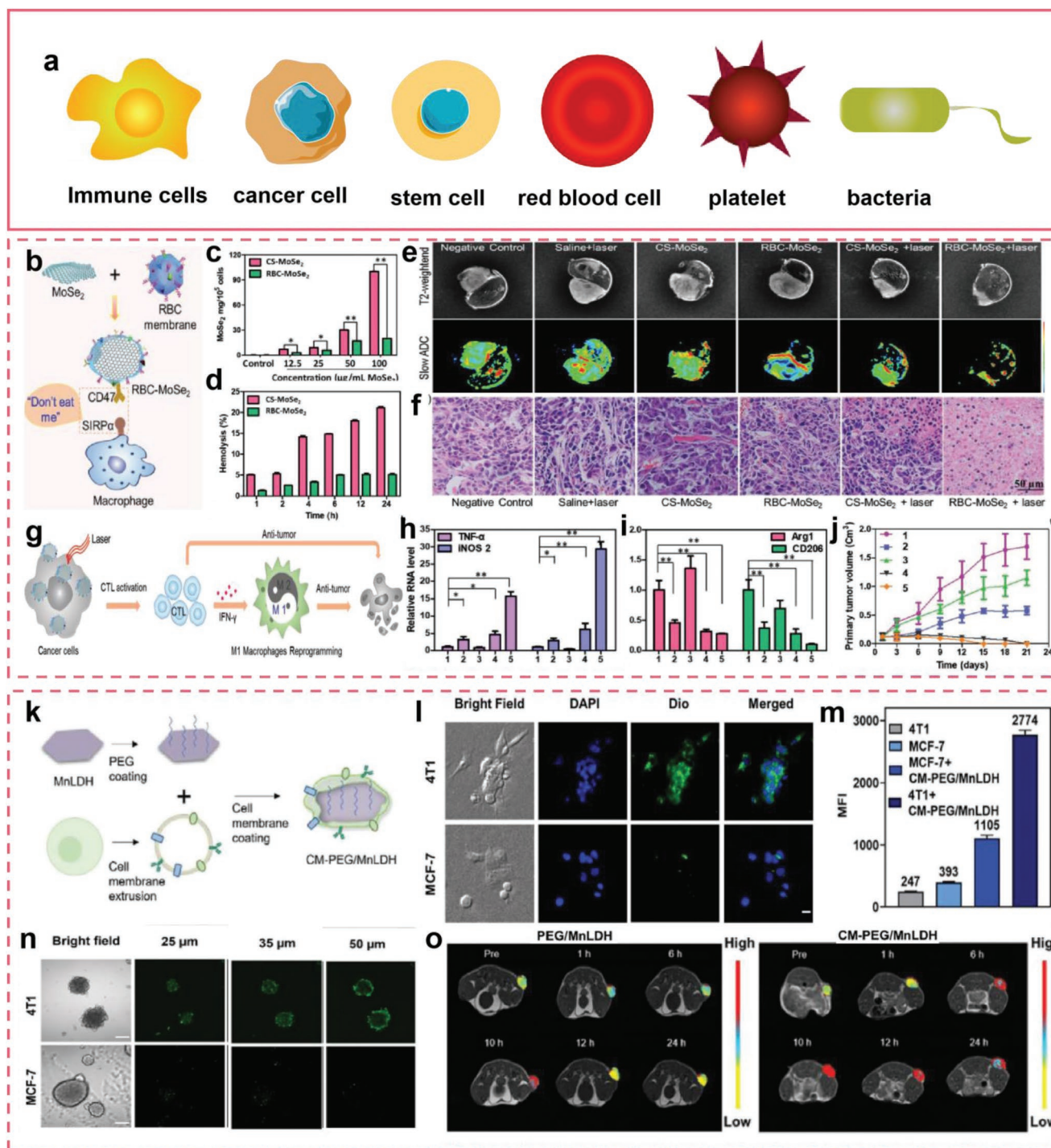
Figure 4. Cell membrane-coated 2D NMs strategies. a) Common types of membrane sources. b–j) RBC-coated 2D MoSe₂ avoids immune clearance and enhances the synergistic effect of PTT and immunotherapy. Reproduced with permission.[35] Copyright 2019, Wiley-VCH. k–o) Cancer cell membrane coated 2D LDH enhanced tumor targeting and tumor tissue penetration. Reproduced with permission.[38] Copyright 2022, Wiley-VCH.

the nanoparticles, which allowed targeting of homotype cancer cells and improved the efficacy of combination therapy.[39]

Immune cells such as macrophages/monocytes reduce the self-recognition by macrophages, while T cells and NK cells effectively increase circulation time and regulate the immune microenvironment against tumors.[40] Stem cells depend on the

adhesion of lymphocyte function associated antigen 1 to intercellular cell adhesion molecule-1, making them suitable for cell-based drug delivery.[41] Bacterial membranes with a variety of immunogenic antigens and intrinsic adjuvant properties stimulate innate immunity and promote adaptive immune responses, increasing the immune response.[42]

In conclusion, the membrane coating of nanomaterials not only enhances their circulation time, increasing their penetration ability into tumor tissues, but also activates immune responses and further enhances the antitumor effect.

2.2. Optimizing Physical and Chemical Properties of Nanosystems

The physical and chemical properties of nanocarriers, such as their size, shape, and surface affect the fate of the nanocarriers in the body. Passive targeting efficiency can be improved by adjusting the physical and chemical properties of nanosystems.

2.2.1. Surface Modification to Avoid Protein Corona

A number of articles have indicated that proteins in the blood are easily coated on the surface of nanomaterials to form a protein corona, which affects targeting.[43] Mallineni et al. studied the interaction of graphene/graphene oxide (GO) with proteins, and their results showed that both bare GO and graphene could strongly interact with tryptophan, tyrosine, and phenylalanine.[44] The surface modification of nanocarriers can effectively reduce interactions with protein and enhance biocompatibility and passive-targeting efficiency. Common surface modifications use polymers such as PEG, polyacrylamide (PAM), polyacrylic acid (PAA), and polysaccharides such as chitosan (CS) and dextran to modify the carrier (**Figure 5**a). Xu et al. compared the effect of polymer-modified GO on reducing protein adsorption. They prepared a series of derivatives including $GO–NH_2$, GO–PAM, GO–PAA, and GO–PEG. The results showed that the protein composition and content adsorbed by each material differed (Figure 5b), but after normalization, surface modification reduced the total adsorbed protein, which was 90.2% for GO–PAM, 54.3% for $GO–NH_2$, 39.3% for GO–PAA, and 43.9% for GO–PEG relative to that of GO (Figure 5c). IgG is the most important antibody in the immune system and plays a crucial role in clearing invading pathogens. IgG content in the protein corona of the surface-modified material was lower than that of GO, which means that the surface modification of the polymer can reduce its phagocytosis (Figure 5d).[45] **Table 2** displays other examples of surface modifications of 2D NMs to increase biocompatibility and avoid the influence of the protein corona.[174–178]

2.2.2. Adjusting Size, Shape, and Charge to Achieve Optimal Passive Targeting

Tunable Size: The EPR effect is size-dependent. The vascular fenestration of subcutaneous tumors is generally 200 nm–1.2 μm, while the size of gliomas and other tumors is further reduced; thus, the size of the nanosystem should not be too large.[27] The size of renal filtration truncation is reportedly 5.5 nm,[46] and the size of hepatic vascular fenestration is reportedly 50–100 nm.[47] Thus, particles smaller than 5.5 nm are more likely to be excreted in the urine, and particles smaller than 50 nm are more likely to penetrate the endothelium of the

liver. As a result, the optimal size of the nanodelivery system is between 50 and 200 nm. Researchers have developed a variety of 2D NMs that can be adjusted in size. For example, Pandeeswar and Govindaraju designed 2D sheets of promising n-type organic semiconductor naphthalene diimide with a tunable size by controlling their self-assembly propensity. Subtle changes in the form of structural mutations in glycine derivatives resulted in 2D nanosheets with well-defined shapes of distinct length, width, and thickness.[48] Klein et al. reported a method for growing 2D nanosheets of hybrid lead halide perovskites (I, Br, and Cl), with tunable lateral sizes ranging from 0.05 to 8 μm and a maximum quantum yield of 49%, which is conducive to drug delivery and PTT-targeted therapy.[49] Yang et al. first reported the synthesis of independent monolayer and multilayer phenylethyl ammonium lead halide perovskite nanosheets $(PEA)_2PbI_4$ NSs (Figure 5e). Their lateral dimensions could be adjusted by changing the solvent. Yang et al. used three solvents, chlorobenzene (C_6H_5Cl), chloroform $(CHCl_3)$, and dichloromethane (CH_2Cl_2). High polar solvents provided higher saturation of the perovskite precursor, which facilitated the formation of smaller-size perovskite NSs. When $CHCl_3$ (0.259) and CH_2Cl_2 (0.309), which have higher relative polarity compared to that of C_6H_5Cl (0.188) and toluene (0.09), were used, the average transverse size of the obtained $(PEA)_2PbI_4$ NSs further decreased to 190 ± 31 and 103 ± 21 nm, respectively (Figure 5f). In addition, these ultrathin 2D perovskite nanosheets exhibited tunable photoluminescence for different imaging applications (Figure 5g).[50] Not only can the size of adjustable 2D NMs be altered according to target requirements, but they also have a more stable and optimized performance after adjustment.

It is worth noting that large-size particles exhibit better tumor site aggregation but their penetration is poor, while small particles show better tumor tissue penetration and low aggregation. Balancing enrichment and penetration is a critical success factor for targeted therapy, and design of variable-size nanosystems is a promising solution. For example, large particle sizes can be maintained in the blood circulation to maximize EPR-effect enrichment. After reaching the tumor site, the nanoparticles can be cleaved into small-size particles or triggered to release drugs to achieve high tumor-tissue penetration. The pH of tumor tissues is usually 6.5–7.2, being slightly acidic, while endosomes (pH 5.0–6.5) and lysosomes (pH 4.5–5.0) are strongly acidic.[51] A large number of acid-responsive 2D nanoplatforms have been established that show decomposition, size reduction, increased tumor penetration, and drug release under acidic conditions. For example, Chen et al. reported highly dispersed 2D MnO_2 nanosheets for concurrent tumor acidic pH-responsive MRI visualization and drug release. The lamellar material realizes efficient loading and delivery of drugs. Under acidic conditions at the tumor site, rapid cracking of the 2D MnO_2 nanosheets enhances the T1-MRI signal, solid tumor penetration, and drug release, achieving accurate treatment.[52]

Optimal Shape: The shape of the nanoparticles also has an effect on the targeting efficiency. Studies have shown that, compared with spherical nanoparticles, nonspherical particles with layered structures roll easier in the vasculature, which greatly increases the tendency of NM-blood vessel wall contact and increases the probability of NMs leaking into tumor sites through

**ADVANCED
SCIENCE NEWS**

www.advancedsciencenews.com

**small
methods**

www.small-methods.com
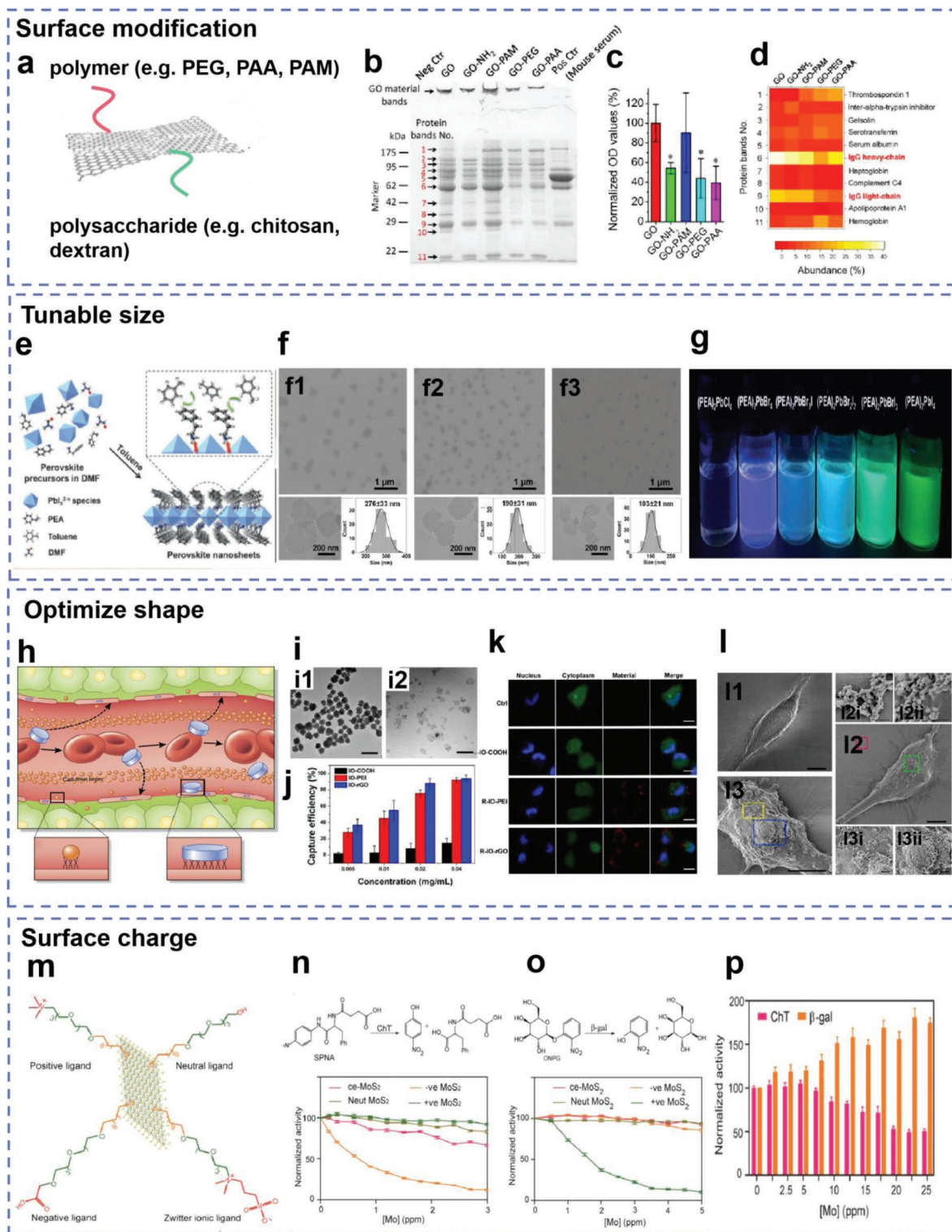
Figure 5. Optimization of physicochemical properties of 2D NMs enhances passive targeting efficiency. a–d) Surface modification such as PEG/PAA/PAM reduces the adsorption of protein and improves the stability of the material. Reproduced with permission.[45] Copyright 2016, American Chemical Society. e–g) Tunable size 2D NMs achieve the optimal balance of tumor aggregation and penetration, and display different wavelengths of photoluminescence. Reproduced with permission.[50] Copyright 2017, Wiley-VCH. h–l) Sheet structure is a more efficient delivery system. h) Reproduced with permission.[53] Copyright 2015, Springer Nature. i–l) Reproduced with permission.[54] Copyright 2019, The Royal Society of Chemistry. m–p) Neutral or amphiphilic particles have good biological stability and low cytotoxicity, and can effectively penetrate tumor cell membranes while maintaining the stability of particle properties. Reproduced with permission.[56] Copyright 2018, American Chemical Society.

Table 2. Examples of surface modifications of 2D NMs that avoid the effects of protein corona.

2D NM types	Modified nanomaterials	Results
Graphene based	CS self-assembly forming CS-GO	Decreased the adsorption capacity of bovine serum albumin and lysozyme, enhanced EPR targeting effect[174]
Graphene based	Dextran functionalization of the GO	Prevent hemolysis, reduce toxicity, and increase circulation time[175]
TMDs	MoS$_2$–PEG–CpG (cytosine–phosphate–guanine)	MoS$_2$–PEG–CpG can significantly promote the accumulation of CpG in tumor cells, and PTT can further enhance the immunotherapy[176]
TMOs	2D MnO$_2$-SPs NSs	Can effectively reduce the influence of protein and increase biocompatibility. No obvious damage to the main organs of mice was observed by MnO$_2$-SP NSS 30 days after injection[177]
Single-element 2D NMs	PEGylated flake-shaped BP-AuNP nanohybrid	PEGylated-BP-AuNP nanohybrid showed good biostability and tumor-enhancing targeting ability. No significant organ damage or inflammation was found in the biopsies of major organs after 16 days treatment, while the tumors were significantly smaller in the combination of chemotherapy and photothermal therapy than in the other controls[178]

vascular fenestrations (Figure 5h).[53] He et al. synthesized spherical magnetic nanocomposites (COOH-IO, IO-polyethylene imine (PEI)) and Fe$_3$O$_4$-modified GO nanosheets (IO-rGO). COOH-IO and IO-PEI are negatively and positively charged spherical particles, respectively. IO-rGO and IO-PEI have similar surface charges and magnetization, but different shapes (Figure 5i). The results showed that the positively charged particles had significantly higher cell uptake than the negatively charged particles, but the 2D IO-rGO particles had the highest degree of cell internalization, Similar results were obtained using confocal imaging, further confirming that sheet-like particles were more easily absorbed by cells than spherical particles (Figure 5j,k). The results of scanning electron microscopy showed that IO-rGO forms a monolayer that covers part of the cell membrane and prefers a small bump on the cell surface, while the spherical nanoparticles are more unevenly distributed, suggesting that the sheet structure is a more efficient delivery system (Figure 5l).[54]

Surface Charge: In addition, the surface charge of nanoparticles influences the targeting effect. Positively charged particles have higher cell uptake efficiency but are more toxic and are more likely to nonspecifically attract proteins in the blood circulation, reducing targeted delivery efficiency.[43] Negatively charged particles are absorbed by cancer cells less effectively due to electrostatic repulsion between the particles and cell membranes.[21] Neutral or amphiphilic particles have better biological stability and lower cytotoxicity, and can effectively penetrate tumor cell membranes while maintaining particle stability.[55] Karunakaran et al. studied the interaction of MoS$_2$ with two protein models (chymotrypsin (CHT) and β-galactosidase (β-gal)) with different surface charges (Figure 5m). The results showed that negatively charged MoS$_2$ inhibited CHT activity (Figure 5n), while positively charged MoS$_2$ inhibited β-gal activity (Figure 5o). Neutral MoS$_2$ functionalized with PEG did not affect the activity of either protein, but amphoteric-ion-ligand-functionalized MoS$_2$ inhibited CHT and induced β-gal hyperactivity (Figure 5p). Unfunctionalized MoS$_2$ was not suitable for biological applications.[56] The study showed that different surface charges could affect protein activity, and the possible effect of charge on the protein should be fully considered when designing the carrier.

In conclusion, passive targeting mediated by the EPR effect has been considered the guiding standard for targeted therapy of nanomaterials for many years. From the above discussion, it can be seen that EPR-effect-targeted drug delivery has been shown to be superior to traditional drug delivery in clinical practice, but the overall efficiency is still relatively low and there is much room for improvement. The size, shape, surface charge, and surface modification of the nanosystem have a comprehensive impact on the efficiency of passive targeting. In designing the nanocarrier, all these factors should be fully considered when choosing the optimal design.

3. Active Targeting

Paul Ehrlich envisioned the concept of a "magic bullet," where nanoparticles are targeted to a desired location, often referred to as "active targeting."[57] Typically, ligands are attached to the surface of nanoparticles for identification of specific tumor receptors/antigens and achieving specific and precise tumor recognition of the target. The particle surface is modified with types of targeting ligands, such as antibodies, aptamers, peptides, proteins, and small molecules with specific recognition, and the ligands bind to receptors/antigens, resulting in precise targeting of the NMs to tumors.[58] Moreover, research on targeting different parts of eukaryotic cells, such as the cell membrane, cytoplasm, nucleus, mitochondria, endoplasmic reticulum, and Golgi apparatus, has become a hot topic. This section will discuss the strategies for active targeting of organelles in different locations by 2D NMs.

3.1. Cell-Membrane Targeting

The cell membrane is a lipid bilayer structure that encloses a variety of proteins. It acts as a barrier to the free entry of extracellular substances into cells and provides an independent environment for cell function during the phagocytosis/endocytosis/exocytosis process.[59] A variety of receptors are expressed on the cell membrane, which recognize and bind specific bioactive substances, such as peptides, aptamers, and antibodies, to activate and initiate a series of physical and chemical changes.[60] Protein overexpression on tumor cell membranes or specific expression of a protein receptor is exploited in active targeting.

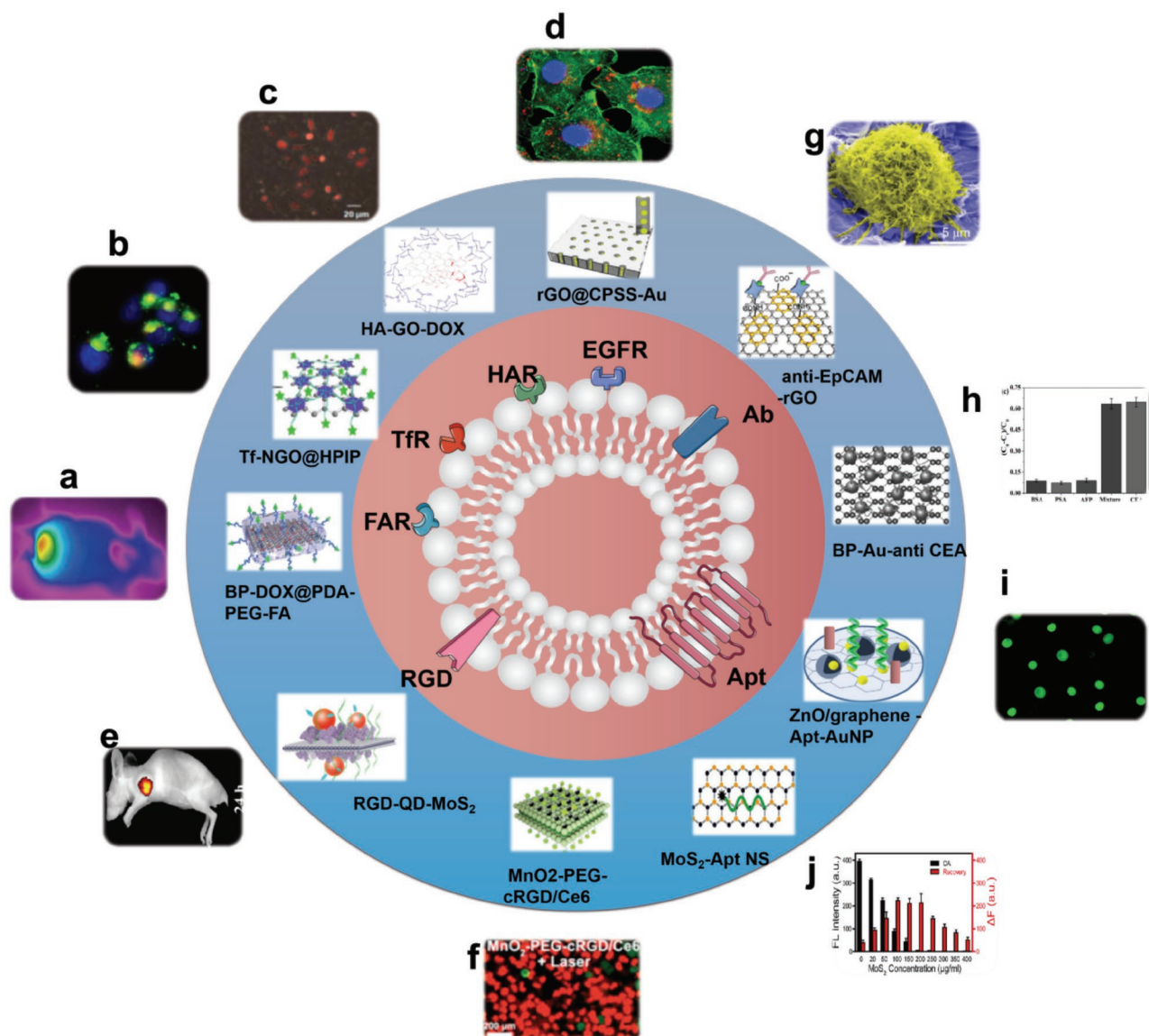#### 3.1.1. Receptor-Mediated Membrane Targeting

Overexpression of a variety of receptors on tumor cell membranes is an important target for active targeting. Folic acid

receptor (FAR), hyaluronic acid receptor (HAR), transferrin receptor (TfR), and epidermal growth factor receptor (EGFR) are membrane receptors overexpressed on various cancer cells, such as lung, breast, ovarian, and prostate cancer cells, which are common target sites.[61]

FAR is overexpressed on the surface of many cancer cells. Shim et al. coloaded camptothecin (CPT) and DOX onto folic acid (FA)-modified GO nanosheets; the CPT and DOX anticancer agents were firmly attached to the FA-conjugated GO via hydrophobic interactions and π–π stacking. DOX/CPT-FA-GO

demonstrated precise and specific targeting to cancer cells and was more lethal to these cells than GO, improving the efficacy of treatment.[62] Gao et al. synthesized one type of BP nanosheet coated with polydopamine and modified with targeting HS-PEG-FA. The nanosheet showed excellent tumor targeting features and antitumor efficacy (**Figure 6**a).[63]

The transport of iron needed by mammals is mainly realized by transferrin and TfR-mediated endocytosis. Studies have revealed that TfR is overexpressed on tumor cell membranes. Some researchers designed TfR-2D NM carriers that achieve

Figure 6. Cell membrane active targeting strategies. a–d) Receptor mediated membrane targeting. a) BP nanosheet targeted FAR. Reproduced with permission.[63] Copyright 2018, American Scientific Publishers. b) Tf-NGO@HPIP targeted TfR. Reproduced with permission.[64] Copyright 2016, Wiley-VCH. c) HA-GO-DOX targeted HAR. Reproduced with permission.[65] Copyright 2014, American Chemical Society. d) rGO@CPSS-Au targeted EGFR. Reproduced with permission.[69] Copyright 2016, Wiley-VCH. e,f) Peptide-mediated membrane targeting. e) RGD-QD-MoS$_2$ targeted RGD. Reproduced with permission.[74] Copyright 2017, The Royal Society of Chemistry. f) MnO$_2$-PEG-cRGD/Ce6 targeted RGD. Reproduced with permission.[75] Copyright 2019, Informa UK Limited. g,h) Antibody-mediated membrane targeting. g) Antibody-EpCAM-rGO binds specifically to EpCAM-positive cells. Reproduced with permission.[77] Copyright 2015, Wiley-VCH. h) BP-Au-antibody CEA binds specifically to CEA. Reproduced with permission.[79] Copyright 2017, Wiley-VCH. i,j) Aptamer-mediated membrane targeting. i) ZnO/graphene–Apt–AuNP targeted S6 Apt. Reproduced with permission.[82] Copyright 2013, Elsevier. j) Apt–MoS$_2$ nanosheets targeted CEA antigen. Reproduced with permission.[83] Copyright 2018, Elsevier.

better targeted therapy in the acidic conditions of the tumor. Zhou et al. constructed a cancer-targeted nano-GO using transferrin as a surface decorator and delivering 2-(4-hydroxyphenyl) imidazo[4,5-f] [1,10]phenanthroline (p-HPIP). The nanosystem was taken up by TfR-mediated cell endocytosis and triggered release of the anticancer agent in acidic environments (Figure 6b).[64]

Hyaluronic acid (HA) is a natural polysaccharide that features in degradable, biocompatible, and nontoxic agents used for various biomedical applications. CD44 receptors are overexpressed on tumor cells. As a ligand of CD44, HA has a high affinity for this receptor. Therefore HA-modified NMs can be targeted to CD44. HA-GO-DOX 2D nanosheets displayed great biostability in culture medium in vitro; these nanosheets could be loaded with large amounts of drug and displayed high targeting efficiency to HepG2 (Figure 6c),[65] A549,[66] and KB[67] cells. In in vivo experiments, HA-GO-DOX displayed higher inhibition of tumor growth rate than free DOX and GO-DOX did.[67]

EGFR is the receptor for epidermal growth factor and has become a new target for tumor therapy. EGFR is also an important cancer biomarker, which can be used to accurately detect cancer through specific binding with ligands.[68] Chen et al. reported a composite NM platform, modified with EGFR, named anti-EGFR-PEG-rGO@CPSS-Au-R6G. This nanocarrier had the ability to amplify Raman signals 5×10^6 times and thus could be used for precise noninvasive cell tracking. Moreover, it displayed high specific targeting of A549 lung cancer cells (Figure 6d).[69] Kim et al. designed a fluorescent probe DNA-GO nanosheet for accurately detecting EGFR exon 19 deletion in nonsmall cell lung cancer.[70]

3.1.2. Peptide-Mediated Membrane Targeting

In the process of tumor proliferation, massive new vessels are formed. The integrin $\alpha_v\beta_3$ is a cell adhesion molecule, which is highly expressed in a variety of tumor cells.[71] Arginine–glycine–aspartic acid (RGD) peptide has high affinity for $\alpha_v\beta_3$; therefore, a 2D nanoplatform modified with RGD was designed to target $\alpha_v\beta_3$ at tumor sites.[72] rGO-PEG-Cy7-RGD[73] was utilized for fluorescence imaging localization and precise tumor targeting of human glioblastoma U87MG tumors. The in vivo imaging results revealed that RGD-modified NMs had higher tumor uptake than GO. Meanwhile, the two nanosheets exhibited highly efficient near-infrared (NIR) PTT performance, resulting in excellent tumor ablation. Some other 2D NMs, such as RGD-QD-MoS$_2$ (Figure 6e)[74] and MnO$_2$-PEG-cRGD/Ce6 (Figure 6f)[75] nanosheets, also demonstrated high tumor targeting and therapeutic effects.

3.1.3. Antibody-Mediated Membrane Targeting

Antibodies are proteins that can bind precisely to their corresponding antigens. Antibodies can be conveniently prepared and have high specificity. Tumor cells express specific antigens; therefore, the interaction between antigen and antibody can be exploited for specific tumor targeting and accurate detection of

tumor biomarkers. Epithelial cell adhesion molecule (EpCAM) is overexpressed in a variety of tumor types, circulating tumor cells, and tumor stem cells.[76] Li et al. designed GO nanosheets modified with anti-EpCAM antibody to capture circulating tumor cells. They tested EpCAM-positive human breast cancer (MCF-7) and human prostate cancer (PC3) cell lines, as well as EpCAM-negative human T (Jurkat), Burkitt's lymphoma (Daudi), and cervical cancer (HeLa) cell lines. After a 45 min incubation period, the capture yields of MCF-7 and PC3-3 cells increased significantly, reaching 92% and 83%, respectively. By contrast, less than 5% of the EpCAM-negative cells Jurkat, Daudi, and HeLa were captured (Figure 6g).[77] Carcinoembryonic antigen (CEA) is a widely accepted tumor biomarker both distributed in the cancer cell membrane and organelles for protein synthesis and transport in the cytoplasm.[78] Peng et al., using few-layer BPs (FL-BPs) mixed with AuNPs to form FL-BP/AuNPs, found that the activity of the catalyst was inhibited when anti-CEA antibody was adsorbed on the Au surface. When CEA was combined with the anti-CEA antibody, the complex was formed in solution, the antibody-CEA was desorbed from the BP-Au surface, and the catalytic reaction was initiated, thus improving the detection sensitivity of cancer biomarkers (Figure 6h).[79]

3.1.4. Aptamer-Mediated Membrane Targeting

Aptamers (Apts) are oligonucleotides filtered by a screening system of high-affinity exponential enrichment and specific binding to phylogenetic ligands. Apts are widely used because of their advantages of simple synthesis, small molecular weight, high chemical stability, and ease of biochemical modification, especially when used in diagnosis and targeted therapy.[80] Zhang et al. constructed the GO nanosheet-loading core–shell-structure Au nanoparticles, Apt-EGFR, and DOX. These materials showed good biostability and binding specificity to lung cancer cells. Specific binding promoted efficient targeted delivery to EGFR-mutated cancer sites in vivo and high anticancer efficacy compared to that of untargeted controls.[81] Liu et al. described a ZnO/graphene–Apt–AuNP composite for targeting SK-BR-3 cells. In that assay, the S6 Apt allowed measuring from 58 cells mL^{-1} to a wide linear range of 1×10^2–1×10^6 cells mL^{-1}. The good resolution for the target cells verified the high selectivity of the proposed cell sensor (Figure 6i).[82] Other articles reported on Apt–MoS$_2$ nanosheets for targeting CEA antigen (Figure 6j),[83] prostate-specific antigen,[84] and renal cell carcinoma.[85]

3.2. Cytoplasm and Organelle Targeting

3.2.1. Targeted Cytoplasm Delivery of Small Interfering (siRNA)

RNA interference (RNAi) refers to the specific degradation of homologous mRNA by siRNA, thereby inhibiting or shutting down the expression of specific genes for therapeutic purposes.[86] RNAi relies on the effective delivery of siRNA into the cytoplasm to react with mRNA. However, naked siRNA itself has strong electronegativity, a large molecular weight, strong

polarity, a short half-life, and is easily removed by endogenous catabolic enzymes and glomerular filtration, severely limiting delivery efficiency. 2D NMs are considered to be excellent cytoplasm-targeted gene-delivery carriers due to their low toxicity, high loading rate, and good biocompatibility.

Yin et al. used FA/MoS$_2$ as nanovectors to deliver HDAC1 and KRAS siRNA to Panc-1 cancer cells. Fluorescence signals indicated that the two types of siRNA were successfully transfected into the Panc-1 cells by the nanocycle vector. Moreover, after NIR laser irradiation, the FA-MoS$_2$-siRNA (HDAC1 + KRAS) achieved 78% tumor growth inhibition efficiency.[87] Human telomerase reverse transcriptase (hTERT) is closely related to the occurrence and development of tumors. Chen et al. delivered hTERT siRNA using BP nanosheets (PPBP-siRNA). The PPBP-siRNA significantly increased the uptake of siRNA by cells. Within 4 h, the siRNA had entered lysosomes but then escaped under the action of PEI and entered the cytoplasm. Western blot analysis also showed concentration-dependent downregulation of hTERT, further confirming that PPBP-hTERT siRNA successfully caused gene silencing. The targeting of PPBP-siRNA in vivo was higher than that of free siRNA, indicating that the vector improved siRNA targeting. Examination of pathological sections showed that ppBP-siRNA treatment inhibited tumor growth and metastasis.[88] Glucose and glutamine are two nutrients required for tumor metabolism. Recently, Xu et al. used LDH to deliver siRNA-Kras and siRNA-GLS1 to simultaneously inhibit glucose and glutamine metabolism. After incubation with PANC-1 cells for 1 h, most of the siRNAs were found in the endosome/lysosome, but after 3 h, the siRNAs escaped the endosome/lysosome, and treatment with LDH-siRNAs could effectively reduce the expressions of Kras, GLS1, and GLUT1 (**Figure 7**a).[89]

3.2.2. Nucleus Targeting

As the largest and most important structure in eukaryotic cells, the nucleus is the center of cell genetics and metabolism, and also the source of various diseases such as cancer. Many anticancer drugs, such as DOX, CPT, and cisplatin, act on the nucleus and kill cancer cells by directly damaging or inhibiting topoisomerases involved in DNA replication by inserting nuclear DNA.[90] The use of chemotherapy drugs alone lacks tumor-specific targeting and causes serious damage to normal cells. Using nanomaterials as delivery carriers can improve the loading efficiency and precise targeting of drugs to improve the therapeutic effect while reducing side effects, which is a promising therapeutic strategy. Generally, the nuclear pore complexes (NPCs) are ≈9 nm in diameter, so that only sufficiently small molecules (such as small ions and molecules) can
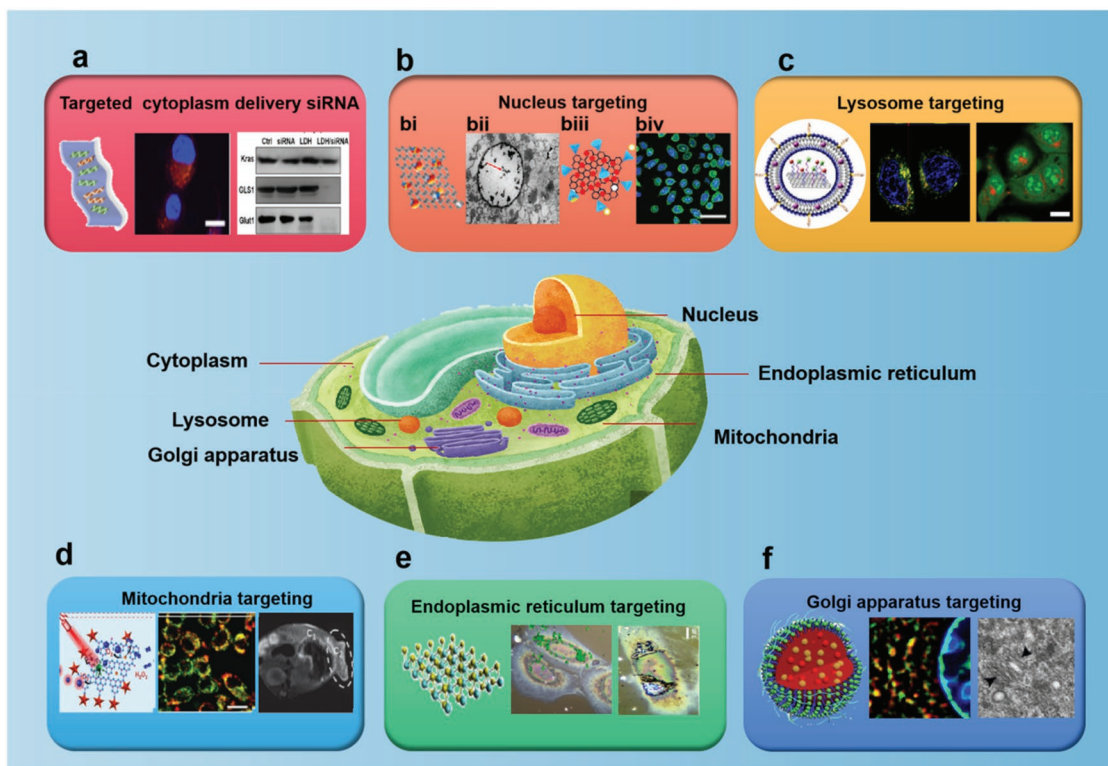
Figure 7. Active targeting subcellular organelle strategies. a) 2D LDH deliver siRNA-Kras and siRNA-GLS1 into the cytoplasm and inhibits glucose and glutamine metabolism. Reproduced with permission.[89] Copyright 2022, American Chemical Society. b) TAT-GO-DOX targeted nucleus delivery of anticancer drugs. bi,bii) Reproduced with permission.[94] Copyright 2019, MDPI. biii,biv) Reproduced with permission.[95] Copyright 2020, Wiley-VCH. c) 2D nanoliposome capsule complex targets the lysosome, causing the lysosome membrane to rupture and producing ROS to kill tumor cells. Reproduced with permission.[101] Copyright 2017, Elsevier. d) 2D Fe^{III}-doped C3N4 nanofusiform targeting mitochondria induced ROS generation. Reproduced with permission.[105] Copyright 2016, Wiley-VCH. e) 2D MoS$_2$ nanosheets targeted the ER. Reproduced with permission.[109] Copyright 2021, American Chemical Society. f) Chondroitin-modified nanomicelles targeted GA. Reproduced with permission.[112] Copyright 2019, American Chemical Society.

passively diffuse into the nucleus.[91] Nuclear localization signals (NLSs) found in polypeptides such as HIV-1 TAT, SV40 T antigen, and various adenoviral proteins have high affinity for NPCs, and nanoplatforms modified with NLSs can effectively deliver the nanocarriers to the nucleus.

Zheng et al. report an anti-HER2 antibody-conjugated poly-ʟ-lysine functionalized reduced GO (antibody-HER2-rGO-PLL) nanocarrier to effectively target DOX to the nucleus of HER2-overexpressing cancer cells. Uptake of this nanocarrier by MCF7/HER2 cells was significantly higher than that of rGO-PLL, due to the specific targeting effect of anti-HER2 on HER2-overexpressing breast cancer cells. In addition, this vector enabled rapid accumulation of DOX in the nucleus, and in vitro cytotoxicity results clearly showed a sevenfold improvement in antibody-HER2-RGO-PLL/DOX efficacy compared to that of RGO-PLL/DOX.[92] TAT-peptide is a commonly used cell-penetrating peptide (CPP), which has high affinity for the nucleus; thus, it has been used to modify peptides targeting the nucleus.[93] Shan et al. constructed a highly efficient nuclear-targeted delivery system of TAT-functionalized GO loaded with the anticancer drug mitomycin C (MMC). Transmission electron microscopy showed that the apoptosis of OCM-1 cells began with the lysis of nuclear material, followed by disappearance of the nuclear membrane and cytoplasm. This indicates that the synthesized MMC-TG is a nuclear-targeted nanodrug that can solve the problem of tumor metastasis from the source (Figure 7bi,ii).[94] Tu et al. developed a circular TAT peptide (CR10) conjugated to polyglycerol-covered GO to engineer a nanoplatform for nucleus-targeted drug delivery. CR10 peptides improved nuclear internalization, while laser irradiation induced the intranuclear release of DOX. In vitro and in vivo experimental results showed that the loaded DOX successfully improved the antitumor effect (Figure 7biii,iv).[95]

3.2.3. Lysosome Targeting

Lysosomes, as an important target organelle, have attracted extensive attention in recent years. External substances enter the cell through phagocytosis, receptor-mediated endocytosis, and other pathways. Lysosomes are dynamically formed in this process and are the link between the internal space of the cell and the extracellular environment.[96] Nanoparticles of different sizes and morphologies enter cells through receptor-mediated endocytosis or pinocytosis, and eventually all accumulate in the lysosome and are exocytosed from the cell by the lysosome.[43] The lysosome contains a variety of hydrolytic enzymes and exhibits strong acidity (pH 4.5–5.0) and increasing evidence shows that lysosomal membrane permeation (LMP) can trigger the cell death pathway.[97] Taking advantage of the acidic conditions to design a pH-responsive carrier to trigger drug release is an effective strategy.

Under acidic conditions, the π–π stacking between DOX and NMs will be weakened, realizing pH-responsive drug release. A pH-responsive charge reversal polyelectrolyte and integrin $\alpha_V\beta_3$ mono-antibody functionalized GO complex was reported. The carrier targets the lysosomes of cancer cells, and the charge reverse stimulation of the polyelectrolyte under acidic conditions effectively releases DOX, which achieves high-dose thera-

peutic effects.[98] Cai et al. reported a composite carrier DOX@Apt–PEG–PDA–MoS$_2$ nanosheet loaded with DOX, coated with a polydopamine (PDA) layer on MoS$_2$, and modified with thiopolymer AS1411 and PEG on MoS$_2$. The AS1411 modification enabled the nanoplatform to target breast cancer MCF-7 cells. The MoS$_2$ and PDA converted 808 nm NIR laser light into thermal energy, which allowed PTT. DOX release was accelerated by the acidic tumor lysosomal environment and NIR laser irradiation. The nanocarrier DOX@Apt–PEG–PDA–MoS2 showed good biocompatibility, a synergistic chemotherapy@PTT effect, and significantly enhanced antitumor efficacy.[99]

Enhanced site-specific release of drugs through photochemical disruption of endosomal/lysosomal membranes has been identified as a key tool for amplifying the outcome of antitumor therapy while minimizing side effects. Zeng et al. designed a targeted drug delivery system modified with branched PEI to load the photosensitizer molecule Ce6 onto a PEI-GO carrier through π–π stacking and hydrophobic interactions. Compared with free Ce6, NGO-PEG-BPEI-Ce6 significantly enhanced the intracellular uptake of Ce6 and targeted lysosomes, resulting in the production of ROS under the excitation of light and achieving highly specific killing of cancer cells.[100] Huang et al. designed a 2D NM-liposome capsule complex that specifically targets tumor lysosomes without irradiation and monitors cell death in real time. Cell colocalization showed that the complex colocalized with lysosomes. LMP-associated cell death was triggered by ROS produced via the artemisinin reaction with ferrous ions (Figure 7c).[101]

3.2.4. Mitochondria Targeting

Mitochondria are the sites where cells produce energy and the main site where cells carry out aerobic respiration.[102] Damage to mitochondria not only affects energy supply, but also produces more ROS and shows a greater tendency to trigger cell apoptosis. Mitochondria are the central organelles of apoptosis; realizing mitochondrial localization in tumor-specific drug delivery systems may be a more effective treatment method. Mitochondria are particularly susceptible to oxidative stress and play an important role in cell death. Photodynamic therapy (PDT) is a method that uses photosensitizers under appropriate irradiation to mediate the death of cancer cells by generating ROS.[103] Mitochondrial-targeted drugs are therefore greatly preferred in PDT.

A mitochondrial-targeted drug constructed with GO was modified with integrin $\alpha_v\beta_3$ monoclonal antibody (mAb), and PEG-conjugated pyropheophorbide-a (PPa) was used to cover the surface of the GO to allow phototoxicity. After the drug enters the cells, it can escape from the lysosome and transfer to the mitochondria. In the mitochondria, the PPa–NGO–mAb showed effective phototoxicity to kill cells. This toxicity involved two steps: 1) cell targeting by the interaction of biological ligands and receptors, and 2) subcellular organelle positioning caused by a physical mechanism that involves the electrochemical reaction between the mitochondrial membrane potential and polarized GO.[104] The PDT process involves the administration of tumor-targeted photosensitizers, which convert localized oxygen (O_2) molecules into highly cytotoxic ROS, especially

ADVANCED
SCIENCE NEWS
www.advancedsciencenews.com

small
methods
www.small-methods.com

singlet oxygen ($^1O_2$), which triggers apoptosis and necrosis under light. However, tumor hypoxia severely limits the efficacy and clinical application of oxygen-depleting PDT. Ma et al. constructed a 2D nano-PDT platform possessing mitochondrial-targeting, H_2O_2-activatable, and O_2-evolving functions based on a 2D Fe^{III}-doped C_3N_4 nanofusiform. Because the surface of the mitochondria is negatively charged, cationic compounds such as triphenylphosphorus (TPP$^+$) have been extensively utilized to achieve targeting to mitochondria. The nanofusiform was transported to mitochondria due to TPP$^+$ modification. Fe^{III} could catalyze the decomposition of H_2O_2, generate O_2 in situ, and then further convert to $^1O_2$. This led to increased PDT potency and ROS concentration in mitochondria, which further enhanced cell death (Figure 7d).[105]

3.2.5. Endoplasmic Reticulum (ER) Targeting

Interfering with the normal function of the ER will cause ER stress. Excessive ER stress will cause cell death, making the ER a potential target for direct cancer suppression.[106] Glycosylation inhibitors, proteasome inhibitors, ER chaperone inhibitors, and ER Ca^{2+}-depleting agents (such as various ionophores and thapsigargin) has been reported to induce cell death through ER stress, some of which have been confirmed to have cytotoxic effects on various cancer cells.[107] Guo et al. used curved 2D NM corannulene (Cor) to achieve dual targeting of the mitochondria and ER for the first time.[108] Cor has unevenly distributed electrons, resulting in a large dipole moment, which is conducive to electrostatic interactions. Cor dipole-induced electrostatic interactions with mitochondria allow initial targeting to mitochondria, followed by transport to the ER through the interconnected structure of the mitochondria and ER. Under light irradiation, electron delocalization of Cor induces the generation of ROS. These two characteristics make Cor the first dual organelle (mitochondria/ER)-targeted substance, showing the potential of subcellular ROS delivery to enhance cancer treatment. Recently, using an ultrathin film substrate, the internalization of MoS$_2$ nanosheets was achieved through mechanotransduction for the first time. Interestingly, volumetric Raman diagrams showed that the material localizes to the ER. In this work, substrates stimulate cell membrane proteins to perceive and recognize them, triggering uptake pathways. This work confirmed a new technology of targeted receptor-mediated uptake that has practical potential in the field of ER-targeted therapy, and its connection with the ER was verified (Figure 7e).[109]

3.2.6. Golgi Apparatus (GA) Targeting

The GA plays a central role in the secretory pathway, processing proteins and then sorting them to specific parts of the cell or secreting them outside the cell.[110] GA not only plays a key role in the reception, modification, packaging, and transportation of proteins and lipids, but also participates in a series of cellular processes. Recent studies have determined that the GA is the hub of signaling molecules in the process of metastasis, especially those related to migration, invasion, and angi-

ogenesis.[111] Therefore, the GA may be closely related to the metastasis and spread of tumors, and destroying the structure of the GA in tumor cells may be a potential method to suppress tumor metastasis. There are two main strategies for GA targeting: 1) modify compounds with high affinity for the GA such as benzenesulfonamide, cysteine, and chondroitin sulfate on the surface of the materials (Figure 7f),[112] and 2) use modifications to avoid the lysosomal pathway and directly transfer to the GA, such as using Shiga toxin, Shiga-like toxins, ricin, cholera toxin, *Escherichia coli* heat-labile toxin, and *Pseudomonas* exotoxin that can enter cells through clathrin-dependent or clathrin-independent endocytosis and directly target the GA.[113] However, research on 2D NMs targeting the GA is still lacking. Researchers should pay more attention to GA targeting.

In conclusion, all parts of the cell play unique and important functions. To achieve the purpose of accurately killing tumor cells, the design of delivery systems that actively target different subcellular parts is an effective method to accurately induce cell apoptosis. Active-targeting therapeutic strategies are more specific at targeting tumor tissue than the EPR effect, improving targeted cell recognition and targeted cell uptake.

4. TME-Related Targeting

The TME is a complex system that refers to the unique ecological environment formed in the process of tumor growth. The TME is very different from the environment of normal tissues, including not only the structure, function, and metabolism of tumor tissues, but also the internal environment of tumor cells. Through clinical observations of organ-specific metastasis of breast cancer, in 1889, Paget put forward the new concept of "seed and soil" and indicated for the first time that TME played an key role in the process of tumor metastasis, which should not be ignored.[114] The TME has a unique biochemical environment, such as low pH, hypoxia, and elevated hydrogen peroxide (H_2O_2) and glutathione (GSH) levels, which is quite different than the normal tissue environment.[115] Meanwhile, the complex immunosuppressive network formed by stromal cells, inflammatory cells, the vascular system, extracellular matrix (ECM), immune-related cells, and their secreted cytokines in the TME plays a key role in tumor immune escape (**Figure 8**). To take advantage of the special TME of tumors to design tumor-targeted therapy vectors, remolding the TME has become a research hotspot.[116] Targeting strategies involving the TME are mainly aimed at four aspects: 1) utilizing or improving the specific physiological environment of the TME to achieve the purpose of tumor-targeted therapy, 2) relieving the immunosuppressive environment of the tumor, 3) destroying or normalizing the tumor's abnormal vascular system, and 4) remodeling the ECM system.

4.1. Targeting Physiological Conditions in the TME

4.1.1. High GSH Levels

GSH is thiol-containing peptide, which regulates cellular redox levels and is found mainly in the mammalian cytoplasm at high

ADVANCED
SCIENCE NEWS
www.advancedsciencenews.com

small
methods
www.small-methods.com
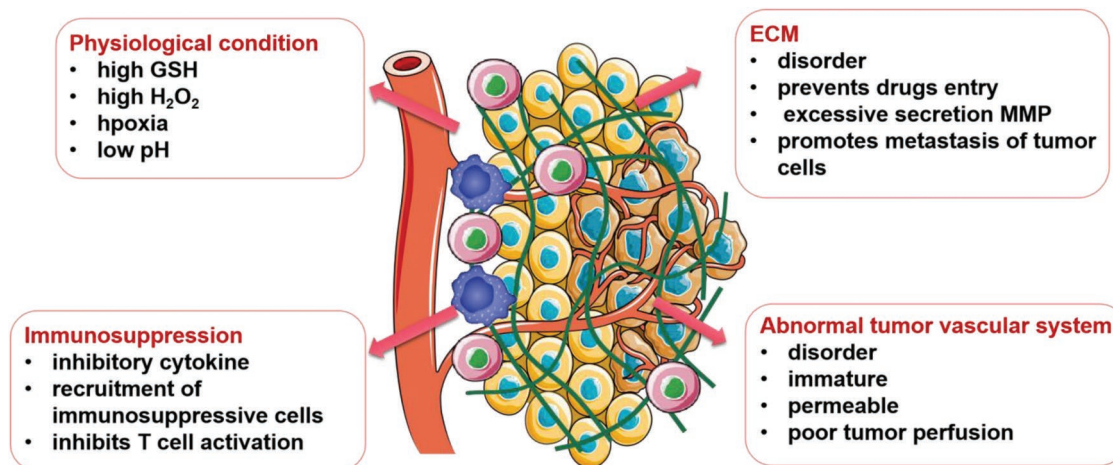
Figure 8. Physiological characteristics of TME.

concentrations. The level of GSH can effectively regulate oxidative stress; therefore, it is considered an effective new target. The quantity of GSH is at least fourfold higher in tumor cells than in normal tissues. Therefore, GSH is being investigated as a novel trigger for tumor-targeted drug delivery and detection.[117] For example, Guo et al. synthesized GO-MnO$_2$ fluorescein (GO-MnO$_2$ FL) nanocomposites for the detection of GSH. The working principle was that GSH can reduce MnO$_2$ to Mn^{2+} and block the energy transfer between FL and GO-MnO$_2$, resulting in significantly enhanced FL fluorescence. When it detected GSH levels in the TME, the nanocomposite fluoresced to selectively image cancer cells. This nanocomposite has great potential in GSH-mediated cancer diagnosis (**Figure 9**a(i)).[118] In addition to detecting cancer cells via consuming GSH, the tumor can be treated. For example, Chen et al. prepared a PEI–SS–DOX–AgNPs–GO nanosheet, where high intracellular GSH levels break the disulfide bonds and release DOX, while DOX fluorescence and surface-enhanced Raman scattering imaging of the AgNPs can allow monitoring of intracellular drug release and vector localization.[119] Gao et al. proposed a 2D platinum delivery platform based on MnO$_2$ nanosheets. On the one hand, it can inhibit Pt-based drug efflux caused by drug-resistant proteins; on the other hand, MnO$_2$ consumes GSH and reduces the formation of GSH-Pt complexes to achieve synergistic treatment to improve the therapeutic effect.[120] Dong et al. designed ultrathin 2D PEG-Bi$_2$MoO$_6$ nanosheets, which had an anoxic structure by consumption of GSH and could promote the separation of electron hole pairs. Ultrasound introduced mechanical strain into the nanoribbons, leading to piezoelectric polarization and band bias, thus accelerating the generation of toxic ROS (Figure 9a(ii)).[121]

4.1.2. Hypoxia

The environment of solid tumors is hypoxic. Studies have confirmed that this hypoxic environment promotes the invasion and metastasis of tumors, and inhibits the tumor therapeutic effect.[122] Excessive secretion of H$_2$O$_2$ in the tumor seriously influences the generation of toxic ROS; reduces the therapeutic

effect of chemotherapy, radiotherapy, and PTT; and further promotes the proliferation and transformation of cancer cells.[123] In recent years, researchers have developed a variety of strategies for dealing with hypoxia. There are three main strategies: 1) reduce hypoxia by generating oxygen at the tumor site, 2) deliver hypoxia-sensitive drugs, and 3) explore other effective therapeutic agents or free radical promoters capable of maintaining high levels of cytotoxic free radicals, independent of oxygen levels in the TME. Therefore, a series of 2D NMs were designed for precise targeting and treatment of tumor hypoxic conditions.

The catalytic decomposition of H$_2$O$_2$ at the tumor site to produce oxygen is a common strategy. MnO$_2$ and CaO$_2$ nanoparticles can be used to break down H$_2$O$_2$ into O$_2$. Lim et al. synthesized MnO$_2$–FA–GO composite nanosheets, where MnO$_2$ decomposes H$_2$O$_2$ to produce oxygen to achieve good PTT combined with an enhancement effect of reduced hypoxia.[124] Tao et al. designed an rGO–MnO$_2$–PEG nanosheet, where the dissolution of MnO$_2$ under acidic conditions and the catalytic pathway of H$_2$O$_2$ decomposition directly produce a large amount of Mn^{2+}, which is used as an MRI contrast agent. The ^{131}I-labeled rGO–MnO$_2$–PEG nanocomposite achieved good tumor killing during in vivo tumor radioisotope therapy (Figure 9bi-1).[125] Gao et al. constructed 2D Nb$_2$C–IO–CaO$_2$ nanoreactors using CaO$_2$ as a strong electron donor for H$_2$O$_2$ to maintain the catalytic Fenton reaction mediated by the IO nanoparticles and release highly toxic hydroxyl radical to induce tumor cell apoptosis. Meanwhile, the photothermal effect further promoted the generation of hydroxyl radical in the tumor, and the nanoreactor significantly increased the production of ROS, which synergistically improved the therapeutic effect (Figure 9bi-2).[126]

Hypoxia makes producing ROS difficult but may be beneficial for some hypoxic-sensitive drug delivery systems. The potential for conversion of nitroimidazoles to hydrophilic imidazoles under hypoxic conditions makes them extremely attractive for cancer hypoxia imaging and hypoxic-responsive drug preparation.[127] Yang et al. developed a layered multifunctional GO drug-delivery system for codelivery of metronidazole (MI), 5-fluorouracil (5-FU), and FePt magnetic nanoparticles. MI
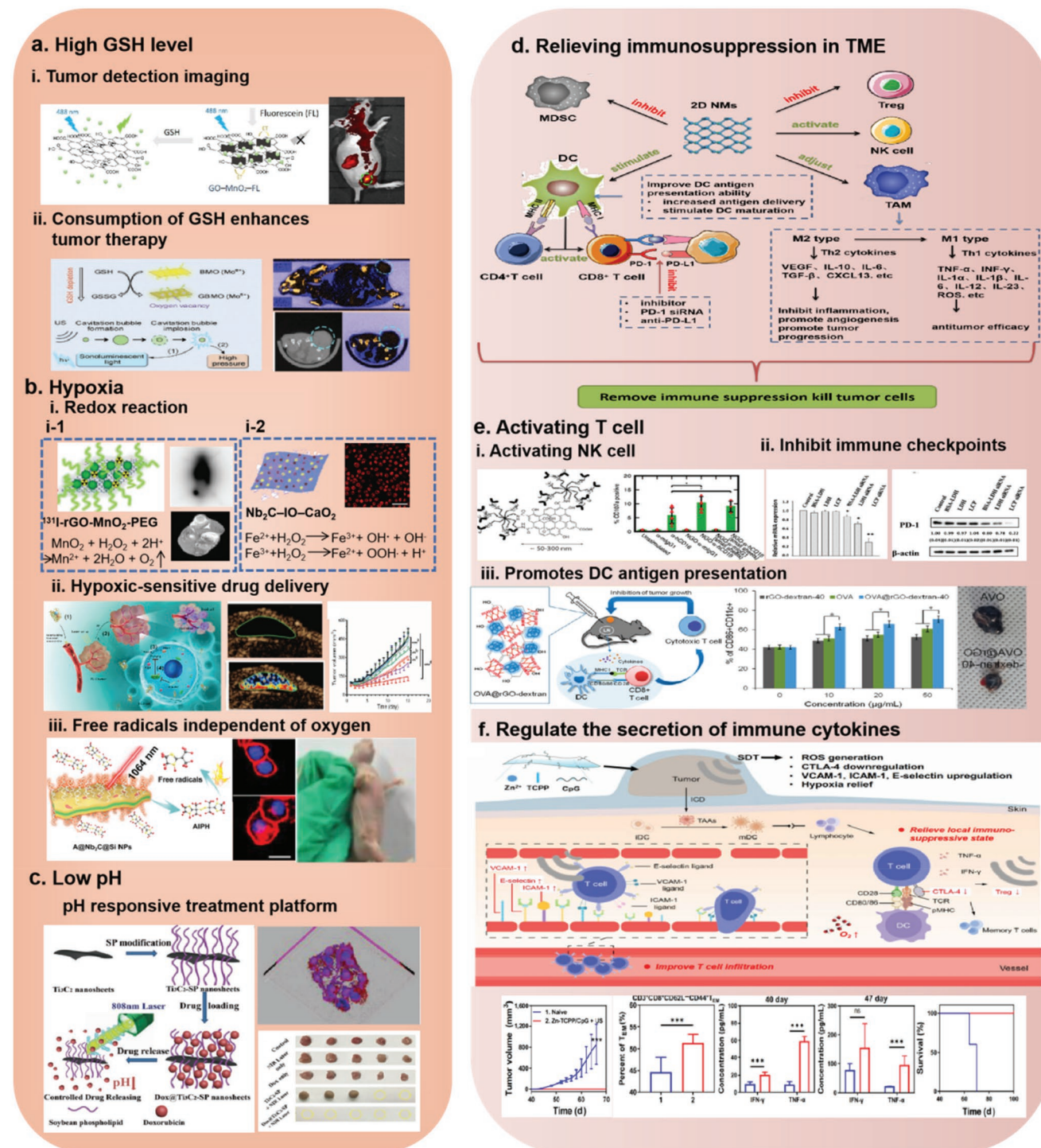
Figure 9. a–c) Target physiological conditions in TME. a) GSH responds to monitoring and enhancement of tumor therapy. ai) Tumor detection imaging. aii) Consumption of GSH enhances tumor therapy. ai) Reproduced with permission.[118] Copyright 2018, Elsevier. aii) Reproduced with permission.[121] Copyright 2021, Wiley-VCH. b) Targeted therapy strategies for tumor hypoxia. bi) Redox reaction. bii) Hypoxic-sensitive drug delivery. biii) Free radicals independent of oxygen. bi-1) Reproduced with permission.[125] Copyright 2018, The Royal Society of Chemistry. bi-2) Reproduced with permission.[126] Copyright 2019, The Royal Society of Chemistry. bii) Reproduced with permission.[129] Copyright 2018, Wiley-VCH. biii) Reproduced with permission.[130] Copyright 2019, American Chemical Society. c) pH sensitive delivery carrier. Reproduced with permission.[134] Copyright 2018, Wiley-VCH. d–f) Targeted regulation of the immunosuppressive environment in the TME. d) Multiple strategies for alleviating immunosuppression in TME. e) Reactivating T cell strategies. ei) Activating NK cell. eii) Inhibit immune checkpoints. eiii) Promotes DC antigen presentation. ei) Reproduced with permission.[161] Copyright 2018, American Chemical Society. eii) Reproduced with permission.[162] Copyright 2019, MDPI. eiii) Reproduced with permission.[163] Copyright 2017, American Chemical Society. f) Regulate the secretion of immune cytokines. Reproduced with permission.[164] Copyright 2021, Springer.

ADVANCED
SCIENCE NEWS
www.advancedsciencenews.com

small
methods
www.small-methods.com

has the ability to assist the action of radical anions to cause DNA damage during irradiation, and 5-FU obstructs the repair of sublethal DNA damage and significantly improves the efficiency of radiotherapy at the biological level. Therefore, the codelivery of MI and 5-FU can have an additive effect on cytotoxicity and radiotherapy, thereby coenhancing radio-chemotherapy. Recently, using a 2D MOF as the main body, a modified catalase-mimicking Pt nanozyme and photosensitizer was designed. The nanoenzyme could catalyze H_2O_2 to generate oxygen, and under the action of the photosensitizer, the oxygen produced was converted into $^1O_2$, which was used to generate ROS, thus enhancing the apoptosis of tumor cells.[128] Luan et al. reported a trimodal tumor vascular-targeted therapy method that exploited hypoxic conditions. They chose GO as the nanovector to efficiently load the photosensitizer verteporfin (VP), banoxantrone dihydrochloride (AQ4N), HIF-1α siRNA (siHIF-1α), and GO modified with c(RGDfK) peptides. The trimodal process was as follows. First, active targeting was adopted to target the tumor site through modification of the c(RGDfK) peptides. Second, the VP photosensitizer could aggravate the hypoxic environment of the tumor under 605 nm laser irradiation. Third, conversion of the AQ4N prodrug into the active AQ4 drug enhanced chemotherapy. Simultaneously, siHIF-1α inhibited HIF-1α expression under hypoxic conditions, further increasing the CYP1A1 and CYP2B6 levels required for AQ4N activation, achieving great therapeutic effects (Figure 9b(ii)).[129]

More recently, researchers have proposed a new strategy to explore other free radical promoters, regardless of the hypoxic environment. As promising molecules, thermal decomposition free radical initiators provide an effective alternative strategy for cancer therapy under normoxic and hypoxic conditions. Xiang et al. reported oxygen-independent free radical-induced cancer cell death using a heat-resistant promoter. 2D Nb$_2$C MXene nanosheets were modified by a mesopore silica layer for loading the initiator 2,2'-azobis[2-(2-imidazolin-2-yl)propane] dihydrochloride (AIPH). Under an NIR-II laser, AIPH was rapidly released and decomposed, generating free radicals and promoting the apoptosis of cancer cells in both normoxic and hypoxic microenvironments. Systematic in vitro and in vivo evaluations have demonstrated the synergistic therapeutic results of this nanoplatform supporting thermodynamic cancer therapy (Figure 9b(iii)).[130]

4.1.3. Low pH

The pH range of tumor tissue is usually 6.5–7.2, being slightly acidic, while endosomes (pH 5.0–6.5) and lysosomes (pH 4.5–5.0) display strong acidity.[131] Taking advantage of the acidic conditions, numerous pH-responsive 2D nanoplatforms have been established to target tumor sites and release anticancer drugs to achieve the goal of precise targeting and treatment. Under acidic conditions, π–π stacking between DOX and NMs is weakened, allowing pH-responsive drug release.[132] Zhang et al. reported on the nanocarrier GO-PAC/HEC that was modified with a mixture of surfactants. DOX was loaded onto the surface of the GO-PAC/HEC with a high loading capacity using the huge specific surface area

and π–π stacking of GO. The in vitro release spectrum of the vector showed significant pH-responsive characteristics and good control of drug release performance. In addition, in vitro studies have shown that DOX-loaded nanoparticles can effectively enter and treat cancer cells and enhance the accumulation of DOX in SKOV3/DDP cells, showing higher cytotoxicity than free DOX.[133] Other 2D NMs also showed the same pH responsiveness. Han et al. studied a new 2D functional material nanosystem (Ti$_3$C$_2$ MXenes), which had high drug-loading capacity and pH-responsive controlled release (Figure 9c).[134] In addition to drug release, many 2D nanodoped materials have pH-sensitive imaging functions, which can be used for diagnostic imaging of tumors. Li et al. developed pH-ultrasensitive Mn-LDH nanoparticles with superb longitudinal relaxivity (9.48 mm^{-1} s^{-1} at pH 5.0 and 6.82 mm^{-1} s^{-1} at pH 7.0 versus 1.16 mm^{-1} s^{-1} at pH 7.4).[135] The vector produces a clear image of the tumor site by responding to pH after injection. A defect-rich multifunctional Cu-doped layered dihydroxide (Cu-LDH) nanosheet was reported. Small Cu-LDH nanoparticles have a large number of defects around the Cu cations and are capable of high photothermal conversion. The Cu-OH octahedron exposed to the LDH surface significantly enhances photothermal conversion (53.1% at pH 7.0% and 81.9% at pH 5.0). This particular Cu microstructure also renders T1-MRI very sensitive to pH, making the material a platform for noninvasive imaging and photothermal therapy.[136]

4.2. Targeted Regulation of the Immunosuppressive Environment in the TME

At the early stage of tumor growth, immune cells recruited and activated by tumor cells and related matrix components can form an inflammatory microenvironment that inhibits tumor development. However, with the continuous proliferation of tumor cells and continuous immune activation response, the TME changes dynamically. Immune effector cells are exhausted or remodeled and unable to perform their normal functions, and the tumor cells utilize the negative regulatory mechanism of the immune system to create an immunosuppressive state. In addition, cancer-associated fibroblast activation, immune cell migration, inhibitory cytokine release, tumor vascular formation, and other factors, forming a wide-ranging immune-inhibitory TME.[137] Regulating the immunosuppressive environment is expected to prevent immune escape and metastatic tolerance of tumors, which has become a hot research direction.

The recruitment of immunosuppressive cells such as regulatory T cells (Tregs), tumor-associated macrophages (TAMs), and bone myeloid-derived suppressor cells (MDSCs) in the TME is one of the main mechanisms for inducing an immunosuppressive TME. The infiltration of Tregs in tumor tissues can directly inhibit the proliferation of effector T cells and produce inhibitory cytokines such as interleukin (IL)-10 and transforming growth factor β (TGF-β), TGF thereby limiting the antitumor immune response and supporting immune escape to promote tumor progression.[138] Usually M1 type macrophages secrete Th1 cytokines and exert proinflammatory and antitumor effects, but the TAM in the TME is M2 type,

which promotes angiogenesis and tumors by secreting Th2 cytokines.[139] TAMs can also induce and maintain immune suppression in the TME by expressing immune checkpoint molecules such as PD-L1, producing immunosuppressive factors such as TGF-β and IL-10, secreting chemokines such as CCL17 and CCL22, and inducing abnormal amino acid metabolism. In addition, TAMs can compete with anti-PD-1 antibody by recruiting Fc receptors on their surface, leading to immune resistance.[140] MDSCs strongly inhibit effector T cells by restricting cysteine necessary for T cell activation, catabolizing arginine necessary for T cell protein synthesis, secreting immunosuppressive factors (e.g., TGF-β), and expressing vascular endothelial growth factor (VEGF) to promote angiogenesis. These effects strongly inhibit effector T cells, natural killer cells, and other activities, and stimulate Tregs, thereby mediating immune escape, which leads to tumor progression.[141] Metabolic remodeling of tumor cells also consumes excessive sugars and amino acids, which competitively deprives T cells of necessary nutrients and promotes T cell dysfunction and immunosuppression.[142] Therefore, there are several strategies for targeted regulation of immune cells: 1) remove immunosuppression and reactivate the immune activity of T cells, and 2) regulate the secretion of immune cytokines (Figure 9d–f).[161–164] In **Table 3**, we summarize the strategies for targeting tumor therapy by modulating the immune environment with 2D NMs.[32,161–164,179–181]

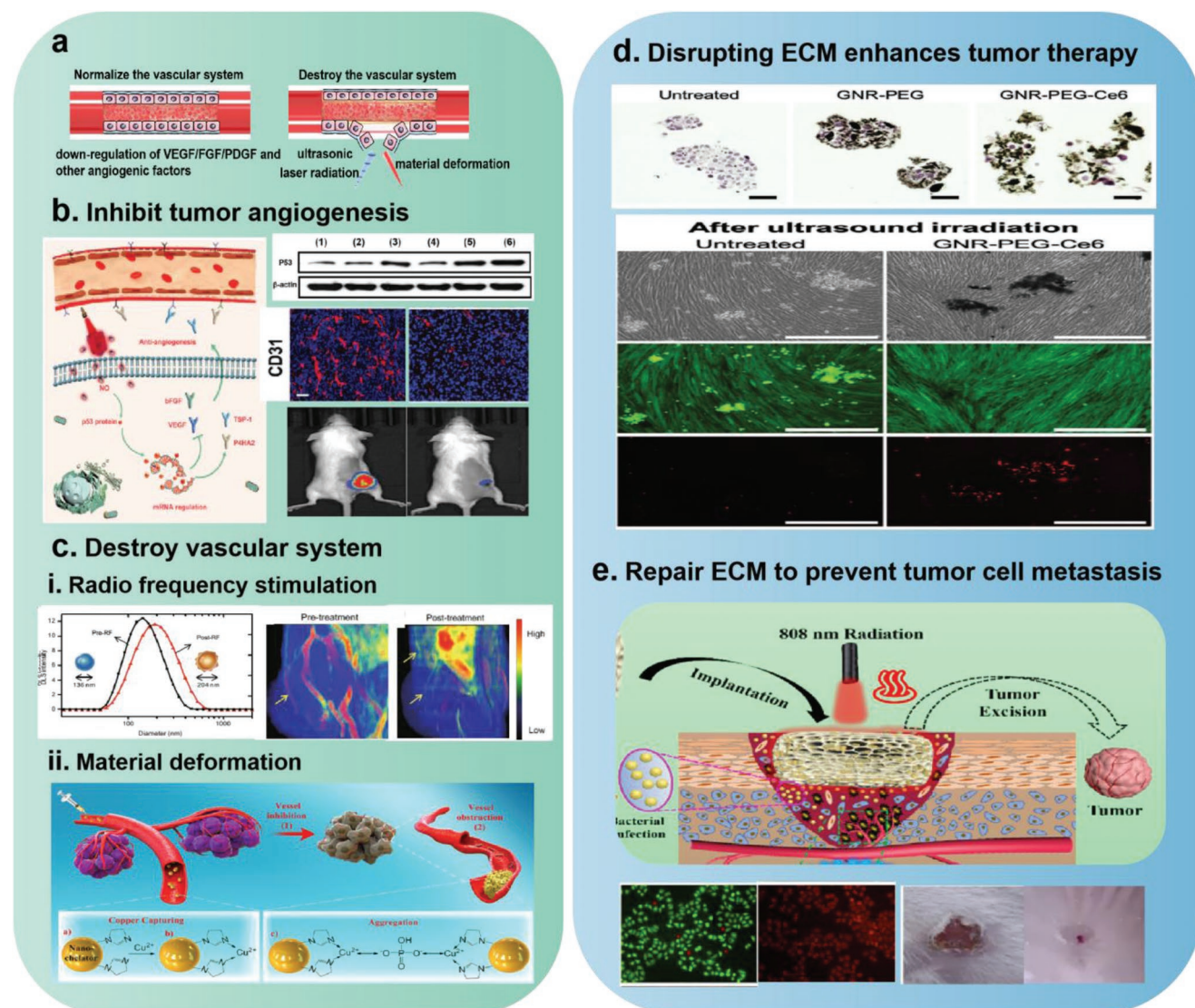### 4.3. Targeted Regulation of Abnormal Tumor Vascular System

The large-scale growth of tumor cells requires blood supply. To obtain this blood supply, tumor cells secrete high levels of angiogenic factors to drive vascular growth.[143] This leads to the formation of abnormal vascular networks, which are characterized by disordered, immature, and permeable vessels, resulting in poor tumor perfusion. An abnormal tumor vascular system leads to hypoxia at the tumor site, hinders the killing effect of immune cells, and leads to further tumor invasion. In addition, abnormal tumor perfusion reduces the diffusion of chemotherapeutic drugs and the efficiency of radiotherapy.[144] Therefore, tumor blood vessels have become an important target for tumor therapy. Destroying or normalizing the abnormal vascular system of tumors is a common strategy for tumor vascular therapy (**Figure 10**a).

Tumor cells can stimulate the secretion of angiogenic factors, such as VEGF, basic fibroblast growth factor (bFGF), and platelet-derived growth factor, and downregulate the production of antiangiogenic factors.[145] Therefore, the antiangiogenesis strategy of tumor targeting aims to promote the activity of antiangiogenic factors and/or reduce the activity of angiogenic factors to inhibit tumor growth and prevent tumor metastasis. The VEGF family of growth factors activates the most important signal pathway regulating angiogenesis. Therefore, a series of studies targeting VEGF have been performed. For example, bovine serum albumin-encapsulated GO has strong binding affinity for VEGF-A165, effectively reduces the content of VEGF in tumor blood vessels, and inhibits the proliferation, migration and tube forming ability of endothelial cells.[146] Li et al. prepared GO-loaded VEGF siRNA. The results showed that it effectively inhibited the growth of tumor tissue and had antiangiogenic activity, which was the result of the downregulation of VEGF protein.[147] Chacko et al. prepared MoS_2–ZnO nanosheets; they found that MoS_2–ZnO specifically activated caspase-3 to induce apoptosis to suppress tumor growth. In addition, the material could downregulate the expression of VEGF, VEGF receptor 2, and other major angiogenesis cytokines to inhibit the formation of blood vessels into the tumor intima.[148] In a recent study, an NIR-II responsive hydrogel was constructed with a nitric

Table 3. 2D NMs target the immunosuppressive environment to reactivate the immune response.

2D NMs	Target	Result
GO	Natural killer cell	They used nanoscale GO to activate natural killer cells. They successfully induced cell activation by stimulating the CD16 NK cell receptor (Figure 9e(i)).[161]
RBC-coated MoSe$_2$ nanosheets	PD-1/PD-L1 pathway; TAMs	He et al. utilized RBC-MoSe$_2$, which could activate the generation of tumor-related antigens, trigger cytotoxic T lymphocytes, silence the PD-1/PD-L1 pathway, and avoid immune escape, and tumor-associated macrophages were effectively reprogrammed into a tumor-killing M1 phenotype.[32]
BP complex	PD-1/PD-L1 pathway	Hanh et al. developed a BP complex including mutated B-raf inhibitors, immune checkpoint (PD-L1) inhibitors, and cancer-targeting antibodies (CXCR4). This complex effectively targeted tumor sites through an active targeting strategy and released PD-L1 inhibitor peptides, leading to a powerful immune response to cure tumors.[179]
LDH	PD-1/PD-L1 pathway	LHD delivering functional PD-1 siRNA to suspended T lymphocytes, successfully reduced the expression of PD-1 in human ex vivo tumor-infiltrating lymphocytes (Figure 9e(ii)).[162]
GO–PEG–PEI	Dendritic cell	Xu et al. designed a GO–PEG–PEI nanosheet carrying urease B as an antigen to promote the maturation of dendritic cells and enhance their cytokine secretion to achieve the purpose of immunotherapy.[180]
FKF-OVAp@BP)	Dendritic cell	The facile coating of BPs with phenylalanine–lysine–phenylalanine (FKF) tripeptide-modified antigen epitopes (FKF-OVAp@BP) enabled the generation of a minimalized nanovaccine by integrating high-loading capacity, efficient drug delivery, and comprehensive dendritic cell activation. Systemic immunization elicited potent antitumor cellular immunity and significantly augmented checkpoint blockade against melanoma in a mouse model.[181]
Dextran-functionalized rGO loading ovalbumin	Dendritic cell	Results showed that rGO–dextran could deliver ovalbumin to dendritic cells efficiently, inducing the release of inflammatory cytokines, and generated T cells in vivo, which had a significant therapeutic effect on the tumor (Figure 9e(iii)).[163]
Zn-TCPP/CpG 2D coordination nanosheets	Regulatory T cells	Zn-TCPP 2D nanosheets exhibiting greatly enhanced ultrasound-triggered ROS generation, significantly improved tumor T cell and regulatory T cell infiltration to enhance antitumor immune responses (Figure 9f).[164]

Figure 10. a–c) Targeted regulation of abnormal tumor vascular system. a) Schematic diagram of targeting tumor vascular system. b) Inhibit tumor angiogenesis. Reproduced with permission.[149] Copyright 2021, Wiley-VCH. c) Destroy the abnormal blood vessels. ci) Radio frequency stimulation. cii) Material deformation. ci) Reproduced with permission.[150] Copyright 2015, Springer. cii) Reproduced with permission.[151] Copyright 2019, American Chemical Society. d,e) Targeted regulation of ECM. d) Disrupting ECM enhances drug penetration. Reproduced with permission.[154] Copyright 2021, Wiley-VCH. e) Repair ECM to prevent cancer metastasis. Reproduced with permission.[157] Copyright 2020, Elsevier.

oxide (NO) precursor (BNN6) and 2D WO2.9 nanosheets were introduced into the hydrogels. The release of NO was activated by laser irradiation. The continuous supply of NO could activate the expression of wild-type p53 protein. p53 protein could inhibit angiogenesis by reducing the transcriptional levels of proangiogenic factors (such as VEGF and bFGF), upregulate antiangiogenic factors (such as thrombospondin 1), and effectively inhibit tumor growth (Figure 10b).[149]

In addition to normalizing blood vessels, destruction of tumor blood vessels is another targeted-therapy strategy. For example, the use of ultrasound, PTT, and other physical methods, could cause the destruction of tumor blood vessels and cut off the nutritional supply of the tumor. Using magnetic metal fullerenes can increase internal energy by absorbing radiofrequency irradiation. After a few minutes to dozens of minutes, due to the increase in internal energy, phase

transformation occurs, accompanied by a dramatic volume expansion of ≈50%, which can destroy the existing tumor blood vessels, disrupt nutritional supply, and kill the tumor (Figure 10c(i)).[150] Yang et al. constructed a nanochelating agent (IMI-OSI, < 6 nm), which chelated copper ions to promote their consumption, thus inhibiting tumor angiogenesis. At the same time, within the TME, the agent aggregated, forming secondary particles and blocking blood vessels (Figure 10c(ii)).[151] There are few studies on the destruction of tumor blood vessels by 2D NMs, which is a promising research direction.

4.4. Targeted Regulation of ECM

The ECM is an important part of the TME. The ECM is mainly composed of collagen, hyaluronic acid, elastin, fibronectin,

laminin, glycoproteins, and proteoglycans; many components combine to form a complete 3D macromolecular network with the cells in tumors.[152] In addition, the ECM stores a large number of cytokines. The lack of tissue oxygenation or the increase in inflammation in the TME induces changes in ECM protein components, resulting in increased ECM density and stiffness. With tumor progression, the ECM becomes more disordered and prevents drugs from entering the tumor tissue. In addition, excessive secretion of matrix metalloproteinases (MMPs) leads to protein hydrolysis and separation of tumor cells from the ECM, leading to the expansion and metastasis of cancer cells.[153] ECM components play an important role in the process of tumor progression, providing continuous proliferation signals for tumor cells, avoiding growth inhibitory factors, resisting cell death, realizing replication immortality, inducing angiogenesis, and promoting invasion and metastasis. Therefore, the ECM has become an important target of tumor therapy. The following paragraphs describe the targeting strategies for the ECM.

When drug therapy is performed at the tumor site, there are often dense ECM limitations. When this occurs, the therapeutic effect can be enhanced by disruption of the ECM, a strategy that has been adopted by some study designs. Lee et al. constructed a PEG-functional graphene nanosheet loaded with Ce6, which destroys the adhesion of ECM proteins to cells, making it easier for tumor cells to adsorb on the nanosheet. The cancer cells that adhered to the nanosheet were then killed with ultrasound. Destruction of the ECM makes it easier for chemotherapy drugs to enter the tumor tissue. Therefore, this material has achieved good tumor-treatment effects (Figure 10d).[154] Su et al. constructed an intelligent 2D BPN-Arg-GOx@MnO$_2$ treatment platform, where a BP nanosheet was modified with L-arginine (L-Arg) and glucose oxidase (GOx), and MnO$_2$ was deposited on the surface. The MnO$_2$ can decompose H$_2$O$_2$ at the tumor site to produce O$_2$, while GOx uses the generated O$_2$ to catalyze the consumption of glucose in cells to produce H$_2$O$_2$. This not only starves the tumor cells, but also promotes the oxidation of L-Arg to NO. NO further increases MMP production and degrades the ECM. The loosened ECM can enhance accumulation of the BAGM nanozyme, thus enhancing the synergistic effect of the photothermal/starvation/NO gas therapy.[155]

By contrast, ECM destruction can promote the migration and invasion of tumor cells. Therefore, some studies have blocked the metastasis of cancer cells by repairing the ECM or depositing a simulated ECM skeleton. Sosnowska et al. added a functional protein cocktail, chicken embryo liver extract protein cocktail, and GOx substrate to a GO plane to increase the expression of adhesion-related genes and decrease the expression of the protooncogene β-catenin to decrease the invasiveness of HepG2 liver cancer cells.[156] On the one hand, the simulated ECM skeleton prepared using the BP photothermal effect showed good photothermal ablation of tumors. On the other hand, released bioactive substances promoted fibroblast proliferation, promoted the expression of genes related to angiogenesis and ECM components of skin tissue regeneration, and accelerated wound healing (Figure 10e).[157]

Mounting evidence shows that tumor occurrence is part of a complex adaptive system involving inflammation, immunity, metabolism, and other factors, and the TME provides "soil" for the occurrence, development, and metastasis of tumors. The complex TME presents challenges and opportunities for efficient drug delivery. For example, the unique physiological environment, which includes acidity and hypoxia, provides favorable conditions for the design of acid-responsive and hypoxia-sensitive delivery systems, while the immunosuppressive environment is not conducive to activation of the immune system. Reasonably designing more efficient and comprehensive 2D NM delivery systems and remodeling the TME are expected to achieve efficient cancer treatment.

5. Conclusions and Perspectives

In 2011, the concept of "precision medicine" was formally proposed by the United States National Research Council. In 2015, US President Barack Obama announced the implementation of the precision medicine plan, which indicated the arrival of a new era of precision medicine. Nonspecific and undifferentiated therapies are now outdated. Precision medicine has new requirements for the precise treatment of diseases, which means that prevention, diagnosis, treatment, and other aspects should be accordingly more targeted and specific to attain the goal of precision treatment. 2D NMs provide a powerful platform for the early realization of precision medicine. Advantages, such as a large specific surface area, make them efficient transfer carriers, and excellent photoelectric and photothermal conversion properties allow them to be used as biological imaging and PTT reagents. In addition, their good biocompatibility and low toxicity enable 2D NMs to have wide applications in tumor diagnosis and treatment.

Research of 2D NMs in precision tumor-targeted therapy involves passive, active, and TME targeting. We have reviewed the design strategies of 2D NMs for precise targeted therapy of tumors, including optimization of physical and chemical properties, surface modification, and regulation of the TEM. Recently, multimode and multifunctional 2D targeted-therapy platforms have also gradually become a trend. For example, theranostic platforms integrating collaborative chemotherapy, PTT, radiotherapy, and imaging diagnosis have been designed and verified to be useful for imaging diagnosis and enhanced tumor treatment.[158,159]

However, the future clinical applications of 2D NMs still face great challenges. The major barrier is their long-term safety, especially for substances that are not biodegradable in vivo. Although many studies have confirmed the short-term safety of 2D NMs, their long-term chronic toxicity remains to be systematically studied.[160] Therefore, it is necessary to strengthen research on the in vivo biological effects of 2D NMs, such as the metabolic pathways, long-term toxicity, and immune responses involved. Optimizing the structure and properties of 2D NMs, improving the biocompatibility of materials, and developing degradable 2D nanoplatforms are promising development directions.

Another major problem limiting clinical application is the low tumor-targeting efficiency of nanoparticles. According to a research paper published in Nature Reviews Materials in 2016, a median of 0.7% of the injected nanoparticle dose actually reached the tumor.[23] The reason for this finding is that once nanoparticles are injected into the body, they face physical and

**ADVANCED
SCIENCE NEWS**

www.advancedsciencenews.com

**small
methods**

www.small-methods.com

biological obstacles (such as agglomeration, protein adsorption, phagocyte isolation, and kidney clearance), which affect the efficiency of the delivery system to reach the target diseased tissues and cells. Strategies that are expected to address these obstacles are mentioned in this review. For example, the biomimetic technology of cell membrane-coated 2D NMs can effectively avoid immune clearance, improve internal circulation time, and increase the percentage of nanoparticles reaching the tumor site. In addition, optimizing the physical and chemical properties of nanosystems, such as their surface modifications, size, and morphology can reduce the adsorption of 2D NMs on proteins and increase their ability to penetrate solid tumors.

In addition to the optimization of delivery system, the dosage threshold of nanoparticles is a new direction worth exploring. A study in 2020 showed that when one trillion nanoparticles were used in mice, a dose exceeding this threshold would reduce the uptake rate of Kupffer cells, nonlinearly decrease liver clearance, prolong the circulation time, and improve the delivery efficiency of nanoparticles to tumor sites up to 12%.[24] These findings form a basic dose-threshold concept for the transport of nanoparticles larger than 10 nm nanoparticles. Future research should study how different nanoparticle designs can improve this threshold and regulate transmission beyond the threshold. Which biological tumor mechanisms dominate to increase the entry of nanoparticles into tumors at high doses should also be studied.

In conclusion, the unique physical and chemical properties of 2D NMs enable them to possess powerful functions of drug delivery, tumor imaging, and tumor therapy, making them promising nanomedicine systems. Strengthening safety research and developing biodegradable materials are key points to accelerate the clinical applications of 2D NMs.

Conflict of Interest

The authors declare no conflict of interest.

[1] D. Albano, M. Benenati, A. Bruno, F. Bruno, M. Calandri, D. Caruso, D. Cozzi, R. De Robertis, F. Gentili, I. Grazzini, G. Micci, A. Palmisano, C. Pessina, P. Scalise, F. Vernuccio, A. Barile, V. Miele, R. Grassi, C. Messina, S. W. G. Young, *Insights Imaging* **2021**, *12*, 76.

[2] D. C. Voshart, J. Wiedemann, P. van Luijk, L. Barazzuol, *Cancers* **2021**, *13*, 367.

[3] J.-L. Meng, T.-Y. Wang, L. Chen, Q.-Q. Sun, H. Zhu, L. Ji, S.-J. Ding, W.-Z. Bao, P. Zhou, D. W. Zhang, *Nano Energy* **2021**, *83*, 105815.

[4] A. G. Olabi, M. A. Abdelkareem, T. Wilberforce, E. T. Sayed, *Renewable Sustainable Energy Rev.* **2021**, *135*, 110026.

[5] L. M. Li, X. L. Jiao, D. R. Chen, C. Li, *Cryst. Growth Des.* **2016**, *16*, 2700.

[6] H. Zhang, L. Zhang, Z. B. Cao, S. S. Cheong, C. Boyer, Z. G. Wang, S. L. J. Yun, R. Amal, Z. Gu, *Small* **2022**, *18*, 2200299.

[7] W. C. Shen, T. T. Hu, X. Y. Liu, J. J. Zha, F. Q. Meng, Z. K. Wu, Z. L. Cui, Y. Yang, H. Li, Q. H. Zhang, L. Gu, R. Z. Liang, C. L. Tan, *Nat. Commun.* **2022**, *13*, 3384.

[8] T. T. Hu, Z. Gu, G. R. Williams, M. Strimaite, J. J. Zha, Z. Zhou, X. C. Zhang, C. L. Tan, R. Z. Liang, *Chem. Soc. Rev.* **2022**, *51*, 6126.

[9] L. Q. Peng, X. Mei, J. He, J. K. Xu, W. K. Zhang, R. Z. Liang, M. Wei, D. G. Evans, X. Duan, *Adv. Mater.* **2018**, *30*, 1707389.

[10] R. Gao, X. Mei, D. P. Yan, R. Z. Liang, M. Wei, *Nat. Commun.* **2018**, *9*, 2798.

[11] W. D. Liu, S. M. Xu, S. Y. Guan, R. Z. Liang, M. Wei, D. G. Evans, X. Duan, *Adv. Mater.* **2018**, *30*, 1704376.

[12] C. Y. Xing, S. Y. Chen, X. Liang, Q. Liu, M. M. Qu, Q. S. Zou, J. H. Li, H. Tan, L. P. Liu, D. Y. Fan, H. Zhang, *ACS Appl. Mater. Interfaces* **2018**, *10*, 27631.

[13] F. Haque, T. Daeneke, K. Kalantar-zadeh, J. Z. Ou, *Nano-Micro Lett.* **2018**, *10*, 23.

[14] L. Cheng, J. J. Liu, X. Gu, H. Gong, X. Z. Shi, T. Liu, C. Wang, X. Y. Wang, G. Liu, H. Y. Xing, W. B. Bu, B. Q. Sun, Z. Liu, *Adv. Mater.* **2014**, *26*, 1886.

[15] J. D. Shao, C. S. Ruan, H. H. Xie, Z. B. Li, H. Y. Wang, P. K. Chu, X. F. Yu, *Adv. Sci.* **2018**, *5*, 1700848.

[16] L. F. Ma, X. R. Song, Y. C. Yu, Y. Chen, *Adv. Mater.* **2021**, *33*, 2008226.

[17] W. Tao, X. Y. Ji, X. B. Zhu, L. Li, J. Q. Wang, Y. Zhang, P. E. Saw, W. L. Li, N. Kong, M. A. Islam, T. Gan, X. W. Zeng, H. Zhang, M. Mahmoudi, G. J. Tearney, O. C. Farokhzad, *Adv. Mater.* **2018**, *30*, 1802061.

[18] L. H. Li, Y. Chen, G. Behan, H. Z. Zhang, M. Petravic, A. M. Glushenkov, *J. Mater. Chem.* **2011**, *21*, 11862.

[19] T. T. Hu, X. Mei, Y. J. Wang, X. S. Weng, R. Z. Liang, M. Wei, *Sci. Bull.* **2019**, *64*, 1707.

[20] Y. Matsumura, H. Maeda, *Cancer Res.* **1986**, *46*, 6387.

[21] M. F. Attia, N. Anton, J. Wallyn, Z. Omran, T. F. Vandamme, *J. Pharm. Pharmacol.* **2019**, *71*, 1185.

[22] J. Shi, P. W. Kantoff, R. Wooster, O. C. Farokhzad, *Nat. Rev. Cancer* **2017**, *17*, 20.

[23] S. Wilhelm, A. J. Tavares, Q. Dai, S. Ohta, J. Audet, H. F. Dvorak, W. C. W. Chan, *Nat. Rev. Mater.* **2016**, *1*, 16014.

[24] B. Ouyang, W. Poon, Y. N. Zhang, Z. P. Lin, B. R. Kingston, A. J. Tavares, Y. W. Zhang, J. Chen, M. S. Valic, A. M. Syed, P. MacMillan, J. Couture-Senecal, G. Zheng, W. C. W. Chan, *Nat. Mater.* **2020**, *19*, 1362.

[25] L. E. van Vlerken, Z. Duan, S. R. Little, M. V. Seiden, M. M. Amiji, *Mol. Pharmaceutics* **2008**, *5*, 516.

[26] J. E. Lancet, G. L. Uy, J. E. Cortes, L. F. Newell, T. L. Lin, E. K. Ritchie, R. K. Stuart, S. A. Strickland, D. Hogge, S. R. Solomon, R. M. Stone, D. L. Bixby, J. E. Kolitz, G. J. Schiller, M. J. Wieduwilt, D. H. Ryan, A. Hoering, M. Chiarella, A. C. Louie, B. C. Medeiros, *J. Clin. Oncol.* **2016**, *34*, 7000.

[27] W. Yu, R. Liu, Y. Zhou, H. Gao, *ACS Cent. Sci.* **2020**, *6*, 100.

[28] W. Yi, K. Wang, G. Cong, Z. He, Z. Hu, T. Chen, J. Liu, X. Tan, T. Tan, M. L. Chang, *Int. J. Hydrogen Energy* **2011**, *36*, 13663.

[29] J. Gallego, G. Varani, *Acc. Chem. Res.* **2001**, *34*, 836.

[30] W. W. Pan, W. J. Chen, Y. Z. Min, J. Wang, Z. Y. Yang, T. Xu, F. Z. Yu, G. D. Shen, Y. Hu, X. P. Ma, *ACS Omega* **2021**, *6*, 35505.

[31] X. Y. Ji, L. L. Ge, C. Liu, Z. M. Tang, Y. F. Xiao, W. Chen, Z. Y. Lei, W. Gao, S. Blake, D. B. De, B. Y. Shi, X. B. Zeng, N. Kong, X. C. Zhang, W. Tao, *Nat. Commun.* **2021**, *12*, 1124.

[32] R. H. Fang, A. V. Kroll, W. Gao, L. Zhang, *Adv. Mater.* **2018**, *30*, 1706759.

[33] Q. Jiang, Y. Liu, R. R. Guo, X. X. Yao, S. Sung, Z. Q. Pang, W. L. Yang, *Biomaterials* **2019**, *192*, 292.

[34] C. M. J. Hu, R. H. Fang, K. C. Wang, B. T. Luk, S. Thamphiwatana, D. Dehaini, P. Nguyen, P. Angsantikul, C. H. Wen, A. V. Kroll, C. Carpenter, M. Ramesh, V. Qu, S. H. Patel, J. Zhu, W. Shi, F. M. Hofman, T. C. Chen, W. W. Gao, K. Zhang, S. Chien, L. F. Zhang, *Nature* **2015**, *526*, 118.

[35] L. He, T. Nie, X. Xia, T. Liu, Y. Huang, X. Wang, T. Chen, *Adv. Funct. Mater.* **2019**, *29*, 1970210.

[36] Y. Lu, X. G. Zhang, X. Q. Hou, M. Feng, Z. Cao, J. Liu, *Nanoscale* **2021**, *13*, 17822.

[37] X. Zhen, P. H. Cheng, K. Y. Pu, *Small* **2019**, *15*, 1804105.

[38] Q. Y. Zhang, D. D. Zhou, G. C. Fang, H. X. Lu, J. F. Zeng, Z. Gu, *Adv. Mater. Interfaces* **2022**, *9*, 2101914.

[39] D. Zhang, Z. Ye, H. Liu, X. Wang, J. Hua, Y. Ling, L. Wei, Y. Xia, S. Sun, L. Xiao, *Nanotheranostics* **2021**, *5*, 275.

[40] A. Parodi, N. Quattrocchi, A. L. van de Ven, C. Chiappini, M. Evangelopoulos, J. O. Martinez, B. S. Brown, S. Z. Khaled, I. K. Yazdi, M. Vittoria Enzo, L. Isenhart, M. Ferrari, E. Tasciotti, *Nat. Nanotechnol.* **2013**, *8*, 61.

[41] H. H. Wu, Y. Zhou, Y. Tabata, J. Q. Gao, *J. Controlled Release* **2019**, *294*, 102.

[42] W. W. Gao, R. H. Fang, S. Thamphiwatana, B. T. Luk, J. M. Li, P. Angsantikul, Q. Z. Zhang, C. M. J. Hu, L. F. Zhang, *Nano Lett.* **2015**, *15*, 1403.

[43] L. Ding, C. Yao, X. Yin, C. Li, Y. Huang, M. Wu, B. Wang, X. Guo, Y. Wang, M. Wu, *Small* **2018**, *14*, 1801451.

[44] S. S. K. Mallineni, J. Shannahan, A. J. Raghavendra, A. M. Rao, J. M. Brown, R. Podila, *ACS Appl. Mater. Interfaces* **2016**, *8*, 16604.

[45] M. Xu, J. Zhu, F. Wang, Y. Xiong, Y. Wu, Q. Wang, J. Weng, Z. Zhang, W. Chen, S. Liu, *ACS Nano* **2016**, *10*, 3267.

[46] H. Soo Choi, W. Liu, P. Misra, E. Tanaka, J. P. Zimmer, B. Itty Ipe, M. G. Bawendi, J. V. Frangioni, *Nat. Biotechnol.* **2007**, *25*, 1165.

[47] L.-T. Chen, L. Weiss, *Blood* **1973**, *41*, 529.

[48] M. Pandeeswar, T. Govindaraju, *J. Inorg. Organomet. Polym. Mater.* **2015**, *25*, 293.

[49] E. Klein, A. Black, Ö. Tokmak, C. Strelow, R. Lesyuk, C. Klinke, *ACS Nano* **2019**, *13*, 6955.

[50] S. Yang, W. X. Niu, A. L. Wang, Z. X. Fan, B. Chen, C. L. Tan, Q. P. Lu, H. Zhang, *Angew. Chem., Int. Ed. Engl.* **2017**, *56*, 4252.

[51] Z. Yang, B. Gu, C. Jiang, L. Zhang, Q. Liu, S. Song, *Nanomedicine* **2021**, *33*, 102356.

[52] Y. Chen, D. L. Ye, M. Y. Wu, H. R. Chen, L. L. Zhang, J. L. Shi, L. Z. Wang, *Adv. Mater.* **2014**, *26*, 7019.

[53] E. Blanco, H. Shen, M. Ferrari, *Nat. Biotechnol.* **2015**, *33*, 941.

[54] Y. He, J. Qin, S. Wu, H. Yang, H. Wen, Y. Wang, *Biomater. Sci.* **2019**, *7*, 2759.

[55] V. Torchilin, *Adv. Drug Delivery Rev.* **2011**, *63*, 131.

[56] S. Karunakaran, S. Pandit, M. De, *ACS Omega* **2018**, *3*, 17532.

[57] A. Hochhaus, P. M. Schlag, N. Cordes, K. Höffken, *Onkologe* **2013**, *19*, 806.

[58] N. Sethulakshmi, A. Mishra, P. M. Ajayan, Y. Kawazoe, A. K. Roy, A. K. Singh, C. S. Tiwary, *Mater. Today* **2019**, *27*, 107.

[59] F. Lang, G. L. Busch, M. Ritter, H. Völkl, S. Waldegger, E. Gulbins, D. Häussinger, *Physiol. Rev.* **1998**, *78*, 247.

[60] D. Zhi, T. Yang, J. Yang, S. Fu, S. Zhang, *Acta Biomater.* **2020**, *102*, 13.

[61] J. Yoo, C. Park, G. Yi, D. Lee, H. Koo, *Cancers* **2019**, *11*, 640.

[62] G. Shim, M. G. Kim, J. Y. Park, Y. K. Oh, *Adv. Drug Delivery Rev.* **2016**, *105*, 205.

[63] N. S. Gao, J. P. Nie, H. F. Wang, C. Y. Xing, L. Mei, W. Xiong, X. W. Zeng, Z. C. Peng, *J. Biomed. Nanotechnol.* **2018**, *14*, 1883.

[64] B. W. Zhou, Y. Y. Huang, F. Yang, W. J. Zheng, T. F. Chen, *Chem. - Asian J.* **2016**, *11*, 1008.

[65] E. Q. Song, W. Y. Han, C. Li, D. Cheng, L. R. Li, L. C. Liu, G. Z. Zhu, Y. Song, W. H. Tan, *ACS Appl. Mater. Interfaces* **2014**, *6*, 11882.

[66] Z. D. Dai, X. Z. Song, J. K. Cao, Y. P. He, W. Wen, X. Y. Xu, Z. Q. Tan, *RSC Adv.* **2018**, *8*, 21975.

[67] W. Miao, G. Shim, S. Lee, S. Lee, Y. S. Choe, Y. K. Oh, *Biomaterials* **2013**, *34*, 3402.

[68] S. Rouhani, N. Yun, C. Bestvina, B. Gilmore, E. Ritz, I. Tarhoni, M. Batus, J. Borgia, P. Bonomi, M. J. Fidler, *J. Thorac. Oncol.* **2021**, *16*, S599.

[69] Y. W. Chen, T. Y. Liu, P. J. Chen, P. H. Chang, S. Y. Chen, *Small* **2016**, *12*, 1458.

[70] D. M. Kim, D. H. Kim, W. Jung, K. Y. Lee, D. E. Kim, *Analyst* **2018**, *143*, 1797.

[71] T. M. Cheng, W. J. Chang, H. Y. Chu, R. De Luca, J. Z. Pedersen, S. Incerpi, Z. L. Li, Y. J. Shih, H. Y. Lin, K. Wang, J. Whang-Peng, *Cells* **2021**, *10*, 1684.

[72] R. N. Liu, F. L. Xu, L. Wang, M. X. Liu, X. Y. Cao, X. Y. Shi, R. Guo, *Nanomaterials* **2021**, *11*, 394.

[73] O. Akhavan, E. Ghaderi, *Small* **2013**, *9*, 3593.

[74] Y. Q. Zhang, W. J. Xiu, Y. T. Sun, D. Zhu, Q. Zhang, L. H. Yuwen, L. X. Weng, Z. G. Teng, L. H. Wang, *Nanoscale* **2017**, *9*, 15835.

[75] D. W. Zeng, L. Wang, L. Tian, S. L. Zhao, X. F. Zhang, H. Y. Li, *Drug Delivery* **2019**, *26*, 661.

[76] Q. J. Wang, Z. Yu, K.-I. Hanada, K. Patel, D. Kleiner, N. P. Restifo, J. C. Yang, *Clin. Cancer Res.* **2017**, *23*, 2267.

[77] Y. Y. Li, Q. H. Lu, H. L. Liu, J. F. Wang, P. C. Zhang, H. G. Liang, L. Jiang, S. T. Wang, *Adv. Mater.* **2015**, *27*, 6848.

[78] Y. Miki, M. Yashiro, K. Kuroda, T. Okuno, S. Togano, G. Masuda, H. Kasashima, M. Ohira, *Cancer Med.* **2021**, *10*, 521.

[79] J. Peng, Y. Q. Lai, Y. Y. Chen, J. Xu, L. P. Sun, J. Weng, *Small* **2017**, *13*, 1603589.

[80] K. Hu, H. Yang, J. Zhou, S. L. Zhao, J. N. Tian, *Luminescence* **2013**, *28*, 662.

[81] M. Zhang, F. Wu, W. T. Wang, J. Shen, N. L. Zhou, C. Z. Wu, *Chem. Mater.* **2019**, *31*, 1847.

[82] F. Liu, Y. Zhang, J. H. Yu, S. W. Wang, S. G. Ge, X. R. Song, *Biosens. Bioelectron.* **2014**, *51*, 413.

[83] L. J. Zhao, M. Cheng, G. N. Liu, H. Y. Lu, Y. Gao, X. Yan, F. M. Liu, P. Sun, G. Y. Lu, *Sens. Actuators, B* **2018**, *273*, 185.

[84] R. M. Kong, L. Ding, Z. J. Wang, J. M. You, F. L. Qu, *Anal. Bioanal. Chem.* **2015**, *407*, 369.

[85] S. H. Zheng, M. Zhang, H. Y. Bai, M. J. He, L. N. Dong, L. L. Cai, M. M. Zhao, Q. Wang, K. Xu, J. J. Li, *Int. J. Nanomed.* **2019**, *14*, 9513.

[86] H. Mok, S. H. Lee, J. W. Park, T. G. Park, *Nat. Mater.* **2010**, *9*, 272.

[87] F. Yin, T. Anderson, N. Panwar, K. Zhang, S. C. Tjin, B. K. Ng, H. S. Yoon, J. Qu, K.-T. Yong, *Nanotheranostics* **2018**, *2*, 371.

[88] L. Chen, C. Chen, W. Chen, K. Li, X. Z. Chen, X. D. Tang, G. F. Xie, X. Luo, X. J. Wang, H. J. Liang, S. T. Yu, *ACS Appl. Mater. Interfaces* **2018**, *10*, 21137.

[89] Y. Xu, Z. Yu, H. Fu, Y. Guo, P. Hu, J. Shi, *ACS Appl. Mater. Interfaces* **2022**, *14*, 21836.

[90] S. Ghosh, S. Mohapatra, A. Thomas, D. Bhunia, A. Saha, G. Das, B. Jana, S. Ghosh, *ACS Appl. Mater. Interfaces* **2016**, *8*, 30824.

[91] A. C. Meinema, J. K. Laba, R. A. Hapsari, R. Otten, F. A. A. Mulder, A. Kralt, G. van den Bogaart, C. P. Lusk, B. Poolman, L. M. Veenhoff, *Science* **2011**, *333*, 90.

[92] X. T. Zheng, X. Q. Ma, C. M. Li, *J. Colloid Interface Sci.* **2016**, *467*, 35.

[93] X. Guo, X. Wei, Z. Chen, X. Zhang, G. Yang, S. Zhou, *Prog. Mater. Sci.* **2020**, *107*, 100599.

[94] S. Shan, S. Jia, T. Lawson, L. Yan, Y. Liu, *Int. J. Mol. Sci.* **2019**, *20*, 4454.

[95] Z. Tu, I. S. Donskyi, H. Qiao, Z. Zhu, W. E. S. Unger, C. P. R. Hackenberger, W. Chen, M. Adeli, R. Haag, *Adv. Funct. Mater.* **2020**, *30*, 2000933.

[96] H. J. Gao, W. D. Shi, L. B. Freund, *Proc. Natl. Acad. Sci. USA* **2005**, *102*, 9469.

[97] H. X. Xu, D. J. Ren, *Annu. Rev. Physiol.* **2015**, *77*, 57.

[98] T. Zhou, X. Zhou, D. Xing, *Biomaterials* **2014**, *35*, 4185.

[99] S. Cai, J. Yan, H. Xiong, Q. Wu, H. Xing, Y. Liu, S. Liu, Z. Liu, *Int. J. Pharm.* **2020**, *590*, 119948.

[100] Y. Zeng, Z. Yang, S. Luo, H. Li, C. Liu, Y. Hao, J. Liu, W. Wang, R. Li, *RSC Adv.* **2015**, *5*, 57725.

[101] L. Huang, Y. Luo, X. Sun, H. Ju, J. Tian, B. Yu, *Biosens. Bioelectron.* **2016**, *92*, 724.

[102] M. P. Murphy, *Biochem. J.* **2009**, *417*, 1.

[103] R. Hilf, *J. Bioenerg. Biomembr.* **2007**, *39*, 85.

[104] Y. Wei, F. Zhou, D. Zhang, Q. Chen, D. Xing, *Nanoscale* **2016**, *8*, 3530.

[105] Z. Ma, M. Zhang, X. Jia, J. Bai, Y. Ruan, C. Wang, X. Sun, X. Jiang, *Small* **2016**, *12*, 5477.

[106] I. Kim, W. J. Xu, J. C. Reed, *Nat. Rev. Drug Discovery* **2008**, *7*, 1013.

[107] Y. Wang, G. Kaur, Y. T. Chen, A. Santos, D. Losic, A. Evdokiou, *ACS Appl. Mater. Interfaces* **2015**, *7*, 27140.

[108] X. Guo, D. Lu, D. Zhang, J. Deng, X. Zhang, Z. Wang, L. Xiao, Y. Zhao, *Mater. Sci. Eng., C* **2020**, *106*, 110227.

[109] R. W. Harries, C. J. Brown, L. Woodbine, A. Amorim Graf, M. J. Large, K. Clifford, P. J. Lynch, S. P. Ogilvie, A. B. Dalton, A. A. K. King, *ACS Appl. Nano Mater.* **2021**, *4*, 2002.

[110] B. S. Glick, A. Nakano, *Annu. Rev. Cell Dev. Biol.* **2009**, *25*, 113.

[111] M. Nishita, S.-Y. Park, T. Nishio, K. Kamizaki, Z. Wang, K. Tamada, T. Takumi, R. Hashimoto, H. Otani, G. J. Pazour, V. W. Hsu, Y. Minami, *Sci. Rep.* **2017**, *7*, 1.

[112] J. Luo, P. Zhang, T. Zhao, M. Jia, P. Yin, W. Li, Z.-R. Zhang, Y. Fu, T. Gong, *ACS Nano* **2019**, *13*, 3910.

[113] M. T. Tarragó-Trani, B. Storrie, *Adv. Drug Delivery Rev.* **2007**, *59*, 782.

[114] S. Paget, *Lancet* **1889**, *133*, 571.

[115] F. Gong, N. Yang, X. Wang, Q. Zhao, Q. Chen, Z. Liu, L. Cheng, *Nano Today* **2020**, *32*, 100851.

[116] S. Thakkar, D. Sharma, K. Kalia, R. K. Tekade, *Acta Biomater.* **2020**, *101*, 43.

[117] F. Meng, W. E. Hennink, Z. Zhong, *Biomaterials* **2009**, *30*, 2180.

[118] Y. Guo, X. Zhang, F.-G. Wu, *J. Colloid Interface Sci.* **2018**, *530*, 511.

[119] H. Chen, Z. Wang, S. Zong, L. Wu, P. Chen, D. Zhu, C. Wang, S. Xu, Y. Cui, *ACS Appl. Mater. Interfaces* **2014**, *6*, 17526.

[120] F. Gao, X. Yang, X. P. Luo, X. L. Xue, C. G. Qian, M. J. Sun, *Adv. Funct. Mater.* **2020**, *30*, 2001546.

[121] Y. Dong, S. Dong, B. Liu, C. Yu, J. Liu, D. Yang, P. Yang, J. Lin, *Adv. Mater.* **2021**, *33*, 2106838.

[122] A. Rapisarda, G. Melillo, *Drug Resist. Updates* **2009**, *12*, 74.

[123] Y. Zhang, H. Liu, X. Dai, H. Li, X. Zhou, S. Chen, J. Zhang, X.-J. Liang, Z. Li, *Nano Res.* **2021**, *14*, 667.

[124] J. H. Lim, D. E. Kim, E. J. Kim, C. D. Ahrberg, B. G. Chung, *Macromol. Res.* **2018**, *26*, 557.

[125] Y. Tao, L. Zhu, Y. Zhao, X. Yi, L. Zhu, F. Ge, X. Mou, L. Chen, L. Sun, K. Yang, *Nanoscale* **2018**, *10*, 5114.

[126] S. Gao, X. Lu, P. Zhu, H. Lin, L. Yu, H. Yao, C. Wei, Y. Chen, J. Shi, *J. Mater. Chem. B* **2019**, *7*, 3599.

[127] H. Liu, Y. Xie, Y. Zhang, Y. Cai, B. Li, H. Mao, Y. Liu, J. Lu, L. Zhang, R. Yu, *Biomaterials* **2017**, *121*, 130.

[128] C. Yang, S. Peng, Y. Sun, H. Miao, L. Meng, S. Ma, Y. Luo, R. Xiong, C. Xie, H. Quan, *R. Soc. Open Sci.* **2019**, *6*, 181790.

[129] X. Luan, Y.-Y. Guan, H.-J. Liu, Q. Lu, M. Zhao, D. Sun, J. F. Lovell, P. Sun, H.-Z. Chen, C. Fang, *Adv. Sci.* **2018**, *5*, 1800034.

[130] H. Xiang, H. Lin, L. Yu, Y. Chen, *ACS Nano* **2019**, *13*, 2223.

[131] J. W. Wojtkowiak, D. Verduzco, K. J. Schramm, R. J. Gillies, *Mol. Pharmaceutics* **2011**, *8*, 2032.

[132] S. Khoee, R. Bafkary, F. Fayyazi, *J. Sol-Gel Sci. Technol.* **2017**, *81*, 493.

[133] Q. Zhang, H. Chi, M. Tang, J. Chen, G. Li, Y. Liu, B. Liu, *RSC Adv.* **2016**, *6*, 87258.

[134] X. Han, J. Huang, H. Lin, Z. Wang, P. Li, Y. Chen, *Adv. Healthcare Mater.* **2018**, *7*, 1701394.

[135] B. Li, Z. Gu, N. Kurniawan, W. Chen, Z. P. Xu, *Adv. Mater.* **2017**, *29*, 1700373.

[136] B. Li, J. Tang, W. Chen, G. Hao, N. Kurniawan, Z. Gu, Z. P. Xu, *Biomaterials* **2018**, *177*, 40.

[137] S. Gao, D. Yang, Y. Fang, X. Lin, X. Jin, Q. Wang, X. Wang, L. Ke, K. Shi, *Theranostics* **2019**, *9*, 126.

[138] A. Gulzar, J. Xu, C. Wang, F. He, D. Yang, S. Gai, P. Yang, J. Lin, D. Jin, B. Xing, *Nano Today* **2019**, *26*, 16.

[139] C. Chen, J.-m. Liu, Y.-p. Luo, *J. Zhejiang Univ., Sci., B* **2020**, *21*, 12.

[140] M. Molgora, M. Colonna, *Med* **2021**, *2*, 666.

[141] K. H. Parker, D. W. Beury, S. Ostrand-Rosenberg, *Adv. Cancer Res.* **2015**, *128*, 95.

[142] B. I. Reinfeld, M. Z. Madden, M. M. Wolf, A. Chytil, J. E. Bader, A. R. Patterson, A. Sugiura, A. S. Cohen, A. Ali, B. T. Do, A. Muir, C. A. Lewis, R. A. Hongo, K. L. Young, R. E. Brown, V. M. Todd, T. Huffstater, A. Abraham, R. T. O'Neil, M. H. Wilson, F. Xin, M. N. Tantawy, W. D. Merryman, R. W. Johnson, C. S. Williams, E. F. Mason, F. M. Mason, K. E. Beckermann, M. G. Vander Heiden, H. C. Manning, et al., *Nature* **2021**, *593*, 282.

[143] C. Viallard, B. Larrivée, *Angiogenesis* **2017**, *20*, 409.

[144] S. M. Weis, D. A. Cheresh, *Nat. Med.* **2011**, *17*, 1359.

[145] A. S. Chung, J. Lee, N. Ferrara, *Nat. Rev. Cancer* **2010**, *10*, 505.

[146] P.-X. Lai, C.-W. Chen, S.-C. Wei, T.-Y. Lin, H.-J. Jian, I. P.-J. Lai, J.-Y. Mao, P.-H. Hsu, H.-J. Lin, W.-S. Tzou, S.-Y. Chen, S. G. Harroun, J.-Y. Lai, C.-C. Huang, *Biomaterials* **2016**, *109*, 12.

[147] J. Li, X. Ge, C. Cui, Y. Zhang, Y. Wang, X. Wang, Q. Sun, *Int. J. Mol. Sci.* **2018**, *19*, 3202.

[148] L. Chacko, A. Poyyakkara, V. Kumar, B. Sameer, P. Aneesh, *J. Mater. Chem. B* **2018**, *6*, 3048.

[149] S. F. Zhao, L. Zhang, L. Deng, J. Ouyang, Q. Q. Xu, X. Y. Gao, Z. L. Zeng, Y. N. Liu, *Small* **2021**, *17*, 2103003.

[150] M. Zhen, C. Shu, J. Li, G. Zhang, T. Wang, Y. Luo, T. Zou, R. Deng, F. Fang, H. Lei, C. Wang, C. Bai, *Sci. China Mater.* **2015**, *58*, 799.

[151] Y. Yang, J. Tang, M. Zhang, Z. Gu, H. Song, Y. Yang, C. Yu, *Nano Lett.* **2019**, *19*, 7750.

[152] M. W. Pickup, J. K. Mouw, V. M. Weaver, *EMBO Rep.* **2014**, *15*, 1243.

[153] Q. Yao, L. Kou, Y. Tu, L. Zhu, *Trends Pharmacol. Sci.* **2018**, *39*, 766.

[154] H. R. Lee, D. W. Kim, V. O. Jones, Y. Choi, V. E. Ferry, M. A. Geller, S. M. Azarin, *Adv. Healthcare Mater.* **2021**, *10*, 2001368.

[155] Y. Su, X. Zhang, L. Lei, B. Liu, S. Wu, J. Shen, *ACS Appl. Mater. Interfaces* **2021**, *13*, 12960.

[156] M. Sosnowska, M. Kutwin, B. Strojny, P. Koczoń, J. Szczepaniak, J. Bałaban, K. Daniluk, S. Jaworski, A. Chwalibog, W. Bielawski, E. Sawosz, *Cancer Nanotechnol.* **2021**, *12*, 2.

[157] Y. Su, X. Zhang, G. Ren, Z. Zhang, Y. Liang, S. Wu, J. Shen, *Chem. Eng. J.* **2020**, *400*, 125949.

[158] W. Chen, J. Wang, W. Du, J. Wang, L. Cheng, Z. Ge, S. Qiu, W. Pan, L. Song, X. Ma, Y. Hu, *ACS Appl. Nano Mater.* **2021**, *4*, 7963.

**ADVANCED
SCIENCE NEWS**

www.advancedsciencenews.com

**small
methods**

www.small-methods.com

[159] K. Zeng, Q. Xu, J. Ouyang, Y. Han, J. Sheng, M. Wen, W. Chen, Y.-N. Liu, *ACS Appl. Mater. Interfaces* **2019**, *11*, 6840.

[160] L. Cheng, X. Wang, F. Gong, T. Liu, Z. Liu, *Adv. Mater.* **2020**, *32*, 1902333.

[161] C. Loftus, M. Saeed, D. M. Davis, I. E. Dunlop, *Nano Lett.* **2018**, *18*, 3282.

[162] Y. Wu, W. Gu, L. Li, C. Chen, Z. Xu, *Nanomaterials* **2019**, *9*, 159.

[163] A. Sinha, B. G. Cha, Y. J. Choi, T. L. Nguyen, P. J. Yoo, J. H. Jeong, J. Kim, *Chem. Mater.* **2017**, *29*, 6883.

[164] W. Zhu, Q. Chen, Q. Jin, Y. Chao, L. Sun, X. Han, J. Xu, L. Tian, J. Zhang, T. Liu, Z. Liu, *Nano Res.* **2021**, *14*, 212.

[165] S. Wang, T. T. Hu, G. Y. Wang, Z. D. Wang, D. Yan, R. Z. Liang, C. L. Tan, *Chem. Eng. J.* **2021**, *419*, 129458.

[166] A. Szuplewska, D. Kulpinska, A. Dybko, A. M. Jastrzebska, T. Wojciechowski, A. Rozmyslowska, M. Chudy, I. Grabowska-Jadach, W. Ziemkowska, Z. Brzozka, A. Olszyna, *Mater. Sci. Eng., C* **2019**, *98*, 874.

[167] S. G. Shi, X. L. Chen, J. P. Wei, Y. Z. Huang, J. Weng, N. F. Zheng, *Nanoscale* **2016**, *8*, 5706.

[168] W. Tao, X. Y. Ji, X. D. Xu, M. A. Islam, Z. J. Li, S. Chen, P. E. Saw, H. Zhang, Z. Bharwani, Z. L. Guo, J. J. Shi, O. C. Farokhzad, *Angew. Chem., Int. Ed. Engl.* **2017**, *56*, 11896.

[169] M. H. Shariare, A. A. Masum, S. Alshehri, F. K. Alanazi, J. Uddin, M. Kazi, *Molecules* **2021**, *26*, 1457.

[170] T. L. Moore, R. Podilakrishna, A. Rao, F. Alexis, *Part. Part. Syst. Charact.* **2014**, *31*, 886.

[171] T. P. Shao, J. Wen, Q. Zhang, Y. W. Zhou, L. Liu, L. H. Yuwen, Y. Tian, Y. L. Zhang, W. Tian, Y. Y. Su, Z. G. Teng, G. M. Lu, J. Xu, *J. Mater. Chem. B* **2016**, *4*, 7708.

[172] T. Liu, S. X. Shi, C. Liang, S. D. Shen, L. Cheng, C. Wang, X. J. Song, S. Goel, T. E. Barnhart, W. B. Cai, Z. Liu, *ACS Nano* **2015**, *9*, 950.

[173] Z. B. Cao, L. Zhang, K. Liang, S. S. Cheong, C. Boyer, J. J. Gooding, Y. Chen, Z. Gu, *Adv. Sci.* **2018**, *5*, 1801155.

[174] T. Yan, H. Zhang, D. Huang, S. Feng, M. Fujita, X.-D. Gao, *Nanomaterials* **2017**, *7*, 59.

[175] S. M. Chowdhury, S. Kanakia, J. D. Toussaint, M. D. Frame, A. M. Dewar, K. R. Shroyer, W. Moore, B. Sitharaman, *Sci. Rep.* **2013**, *3*, 2584.

[176] Q. Han, X. Wang, X. Jia, S. Cai, W. Liang, Y. Qin, R. Yang, C. Wang, *Nanoscale* **2017**, *9*, 5927.

[177] Z. Liu, S. J. Zhang, H. Lin, M. L. Zhao, H. L. Yao, L. L. Zhang, W. J. Peng, Y. Chen, *Biomaterials* **2018**, *155*, 54.

[178] Z. Liu, H. Chen, Y. Jia, W. Zhang, H. Zhao, W. Fan, W. Zhang, H. Zhong, Y. Ni, Z. Guo, *Nanoscale* **2018**, *10*, 18795.

[179] H. T. Nguyen, J. H. Byeon, C. D. Phung, L. M. Pham, S. K. Ku, C. S. Yong, J. O. Kim, *ACS Appl. Mater. Interfaces* **2019**, *11*, 24959.

[180] L. G. Xu, J. Xiang, Y. Liu, J. Xu, Y. C. Luo, L. Z. Feng, Z. Liu, R. Peng, *Nanoscale* **2016**, *8*, 3785.

[181] W.-H. Li, J.-J. Wu, L. Wu, B.-D. Zhang, H.-G. Hu, L. Zhao, Z.-B. Li, X.-F. Yu, Y.-M. Li, *Biomaterials* **2021**, *273*, 120788.

Lin Ding graduated from Shanghai University with a Ph.D. in 2020. During her doctoral study, she went to the University of Michigan Medical School for one-year joint training. After graduation, she entered the First Affiliated Hospital (Shenzhen People's Hospital), Southern University of Science and Technology for postdoctoral research. Dr. Ding is mainly engaged in the design of novel tumor-targeting nanocarriers and development of nanodrugs for the precision diagnosis and treatment of cancer. She has published 20 SCI papers, including 4 SCI papers published in Advanced Materials and Small as the first author/co-first author.

Fu-Rong Li, Researcher, Director of Translational Medicine Collaborative Innovation Center, Shenzhen People's Hospital (The First Affiliated Hospital, Southern University of Science and Technology; The Second Clinical Medical College of Jinan University), Shenzhen, China. His research interests mainly focus on tumor precision medicine and biological efficacy of stem cells. More than 60 articles have been published in SCI included journals such as Cell Research, Journal of Hepatology, and Circulation Research, with a total impact factor of more than 400 points. He has edited and participated in editing three academic works and has obtained six national invention patents.
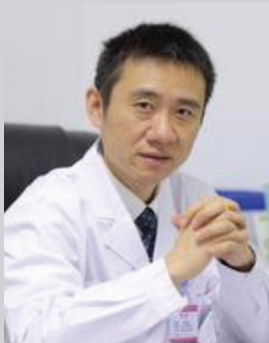
Shuo Gu, Party secretary of the First Affiliated Hospital of Hainan Medical University. Prof. Gu graduated from the Department of Pediatrics, Shanghai Second Medical University in 1997. He has been engaged in clinical work and research in pediatric neurosurgery and has rich clinical experience in the treatment of fetal brain tumors and craniocerebral trauma. He is the 2016 "Good Doctor Introduce Talents" of Hainan Provincial Health and Family Planning Commission and "515 First Level Talents" of Hainan Province. He has published more than 45 papers.

Yanli Wang, Dean of School of Pharmacy, Hainan Medical University, and Director of Hainan Pharmaceutical Research and Development Sci. & Tech. Center. Her main research interests include the application of intelligent targeted nanomaterials in tumor diagnosis and intelligent targeted nanodrug design and its application in tumor therapy. She has presided over four projects of the National Natural Science Foundation of China, including the National Foundation for Outstanding Youth. She has published more than 50 SCI papers in famous international journals such as Nature Communications and Advanced Materials and has applied for 15 invention patents.